IEEE Access
Multidisciplinary | Rapid Review | Open Access Journal

Received February 14, 2019, accepted February 20, 2019, date of publication February 25, 2019, date of current version April 2, 2019.

Digital Object Identifier 10.1109/ACCESS.2019.2901575

Adaptive Trajectory Tracking Control of a Cable-Driven Underwater Vehicle on a Tension Leg Platform

YINGKAI XIA[1,2], (Member, IEEE), KAN XU[3], YE LI[1], (Senior Member, IEEE), GUOHUA XU[2], AND XIANBO XIANG[2], (Member, IEEE)

[1]School of Naval Architecture, Ocean and Civil Engineering, Shanghai Jiao Tong University, Shanghai 200240, China
[2]School of Naval Architecture and Ocean Engineering, Huazhong University of Science and Technology, Wuhan 430074, China
[3]Wuhan Second Ship Design and Research Institute, Wuhan 430205, China

Corresponding authors: Ye Li (ye.li@sjtu.edu.cn) and Guohua Xu (hustxu@vip.sina.com)

This work was supported in part by the National Natural Science Foundation of China under Grant 51479114, Grant 51579111, and Grant 51761135012, in part by the China Postdoctoral Science Foundation under Grant 2018M632117, and in part by the High-tech Ship Research Projects Sponsored by the MIITC Floating Support Platform Project under Grant 201622.

ABSTRACT This paper focuses on the dynamic modeling, controller design, and simulation verification of a new cable-driven underwater vehicle model system, which is proposed for future application on a tension leg platform. Compared with conventional underwater vehicles, the proposed cable-driven underwater vehicle model system has a unique structure and subjects to not only unknown underwater disturbances but also time-varying nonlinear cable tractions. To achieve accurate and robust trajectory tracking control, a universal high-order nonlinear dynamic model is established with multisource uncertainties, and an integrated estimation-based adaptive backstepping terminal sliding mode controller is designed. The proposed controller utilizes the integrated estimation method to handle the multisource unknown uncertainties, where recurrent radial basis function neural network and disturbance observer are employed for the estimations of uncertainties, and adaptive robust methods are utilized for compensations of estimation errors. The backstepping terminal sliding mode control method is utilized to improve the tracking performance and converging rate. In addition, the issue of ''explosion of complexity'' occurred in a traditional backstepping design is tackled by an adaptive control method, and the input saturation problem is solved by anti-windup compensator. Based on the Lyapunov analysis, all closed-loop signals are proved to be uniformly ultimately bounded. The numerical simulations show that the developed controller is not only robust against environmental disturbances and adaptive to unknown time-varying uncertainties but also able to steer the trajectory tracking errors along the prescribed transient, thus leading to effective cable-driven underwater vehicle model system control.

INDEX TERMS Cable-driven underwater vehicle model system, trajectory tracking control, integrated estimation, adaptive backstepping terminal sliding mode control, input saturation.

I. INTRODUCTION

During the past few decades, ocean exploration has experienced a booming development thanks to the advances in marine equipment technology [1], [2]. Among the wide variety of marine equipment, marine platform has become one of the most commonly used structures for offshore exploration and production owing to the excellent structural stability and carrying capability [3], [4]. In order to meet the future application requirements of an underwater tension leg platform, a new cable-driven underwater vehicle model system is proposed in this paper, which is required to perform accurate and robust trajectory tracking control along a pathway on the platform. The current work only focuses on the dynamic modeling, controller design, and simulation verification of the proposed cable-driven underwater vehicle model system, whereas the experiment verification will be addressed in our future works.

Although the proposed vehicle system doesn't have flexible mobility of multiple degrees of freedom compared with conventional underwater vehicles [5], [6], it has better stability and carrying capability due to the cable-driven

The associate editor coordinating the review of this manuscript and approving it for publication was Ali Zemouche.

structure. However, the cable-driven structure brings a lot of nonlinearities and disturbances to the system, making its dynamic behavior more complex. Considering the aforementioned characteristics, accurate and robust trajectory tracking control is quite challenging.

Because of the complex cable-driven dynamic behaviors, building accurate mathematical model of the proposed system is not easy. In the past decades, considerable efforts have been made to describe the complex cable-driven dynamics [7]–[9]. Compared with previous literatures, a general nonlinear mathematical expression is proposed for cable-driven vehicle model system in the current work. Inspired by Lee and Huang [10], the highly nonlinear cable-driven dynamics are expressed as a finite combination of known nonlinear functions in this paper, based on which, a universal high-order nonlinear dynamic model is established with multisource time-varying unknown uncertainties and input saturation.

Considering the complex nonlinearities and multisource time-varying uncertainties, conventional model-based nonlinear control strategies can only give limited performance when accurate and stable trajectory tracking control of cable-driven vehicle is required. Hence, it is important to investigate new effective control method.

Adaptive control based on backstepping technique is one of the most commonly used strategies for a large class of nonlinear systems [11]–[13]. Wu *et al.* [14] proposed a novel adaptive backstepping controller with nonlinear disturbance observer for the longitudinal dynamics of HFV. A novel adaptive backstepping control method was proposed by Butt and Aschemann [15] for nonlinear systems with matched and mismatched unknown parameters. In the work of Luo *et al.* [16], a LS-SVM-based adaptive constrained control scheme was developed under the time-varying predefined performance using backstepping technique.

However, two problems are often encountered when applying the adaptive backstepping technique for complex nonlinear systems. The first one is the parameter uncertainties and unknown external disturbances which could severely degrade the closed-loop system performance and make it hard to obtain explicit control law effectively [17]. The second one is the tedious analytic computations of virtual control laws in the recursive steps, also referred to as ''explosion of complexity'' [18].

To solve the first problem, effective methods must be employed to estimate and compensate for the uncertainties. Neural network [19]–[22] and disturbance observer [23]–[26] have attracted numerous researchers' interests during the past decades. In the work of Zhang *et al.* [27], a robust adaptive backstepping control based on RBFNN was proposed for re-entry attitude tracking control of near space hypersonic vehicle. An adaptive dynamic program (ADP) algorithm based on three neural networks (NNs) was applied to solve the HJI equation [28], based on which, a novel nonlinear control scheme was proposed. In the work of Liu *et al.* [29], kinematics uncertainty in RLFJ robot was first studied by a nonlinear observer, and an adaptive control scheme was proposed. A new fractional-order sliding mode control (FOSMC) based on a nonlinear disturbance observer was proposed to investigate the stabilization and disturbance rejection for fractional-order nonlinear dynamical systems with mismatched disturbances [30]. An extended disturbance observer based sliding mode control method was proposed for general nth order systems with mismatched uncertainties [31]. Recently, some integrated estimation methods based on neural network and disturbance observer have been studied when dealing with complex multisource uncertainties. In the work of Talkhoncheh *et al.* [32], a neural network observer was developed to estimate the unmeasured states, based on which, an adaptive tracking controller was designed. An adaptive tracking controller was developed for a class of strict-feedback nonlinear uncertain systems, on the basis of neural network and disturbance observer [33]. Compared with the single estimation methods, the integrated estimation method improves the anti-jamming ability of the system. However, the coupler design between NN and DO has rarely been considered, which needs to be further investigated.

''Explosion of complexity'' is another significant issue, which is mainly caused by repeated differentiations of the virtual control laws in recursive steps [16], [32]. Especially for high-order nonlinear systems in the presence of unknown disturbances, the derivatives of virtual control variables become more and more tedious considering the growing order of the controlled systems and the unexpected noises and disturbances, which will increase the calculation burdens dramatically and finally ends in the differential explosion. In the existing literatures, many techniques have been employed to solve this problem. Dynamic surface control was utilized by introducing the derivative of first-order filter output instead of conventional intermediate variables [32], [34]–[36]. In the work of Huang and Chen [37], function approximation was used to estimate the uncertainties and derivatives of virtual inputs. In the work of Ginoya *et al.* [24], a disturbance observer was utilized to estimate the derivatives of virtual inputs. In the work of Chen and Ge [38] and Bu *et al.* [39], differentiators were used to exact derivatives of signals.

Another technical challenge for cable-driven vehicle control is the input saturation caused by physical actuator [40]. The undesirable input saturation will influence the stability of the control system and even make the entire system unstable. In many literatures, anti-windup compensators were utilized to reduce the influence of input saturation [41]–[43]. In the work of Chen *et al.* [44], Low gain feedback technique was utilized to achieve the robust consensus of fractional-order multi-agent systems with input saturation and external disturbances. A constrained control allocation was transformed into a convex quadratic programming problem and a recurrent neural network was employed in the work of Chen and Jiang [45], to solve the problem of input saturation.

Motivated by the aforementioned analyses, dynamic modeling and trajectory tracking control of a new cable-driven underwater vehicle model system are addressed in the current

work. To sum up, this paper mainly solves the following three problems:

1) A novel underwater solution with cable-driven vehicle system is provided in the current work, which may expand the future application ideas of the offshore platforms. To the best of the authors' knowledge, such a cable-driven vehicle system has been rarely used in offshore industries.
2) To deal with the multisource unknown uncertainties with unknown upper bounds, an integrated estimation method is employed based on RRBFNN, DO and adaptive robust compensation. Compared with single estimation method, the proposed integrated estimation method has better estimation error compensation and anti-jamming ability.
3) A comprehensive adaptive backstepping terminal sliding mode control method is proposed to ensure the accuracy and robustness of trajectory tracking. Compared with conventional adaptive backstepping control method, more constraints of the system are considered and resolved, i.e., the "explosion of complexity" issue is tackled by adaptive method, and anti-windup compensator is introduced to reduce the influence of actuator saturation.

The remainder of this paper is organized as follows. Section II establishes the universal nonlinear dynamic model and formulates the trajectory tracking control problem. Section III proposes the nonlinear trajectory tracking control scheme, and presents the detailed deriving and proving process of controller design. Section IV validates the previous analysis and design through simulation cases and discussions. Section V demonstrates the conclusions and some future works.

II. MODELING AND PROBLEM FORMULATION

A. SYSTEM MODELING

As shown in Fig. 1, the proposed cable-driven underwater vehicle model system is installed on an underwater tension leg platform. Driven by the hydraulic winch and closed-loop cable-wheel system, the underwater vehicle is regulated to move along a pathway on the platform.

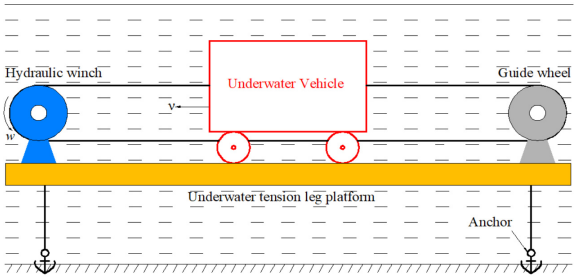

FIGURE 1. The proposed cable-driven underwater vehicle model system.

The proposed cable-driven underwater vehicle model system contains the following important properties:

1) ***Highly nonlinear cable-driven dynamics:*** Although the cable-driven structure has good stability and load carrying capacity, it exhibits high nonlinearity. Especially for the case of insufficient cable stiffness, unexpected cable tension fluctuations are more likely to occur.
2) ***Multisource unknown uncertainties:*** The unmeasured frictions, unknown underwater disturbances, and time-varying hydraulic parameters bring various unknown uncertainties to the system, which could severely degrade the closed-loop system performance and make it hard to obtain explicit control law effectively.
3) ***Input saturation:*** Due to the limited output torque of hydraulic winch, the system suffers from inherent actuator saturation, which may influence the control effect and even make the entire system unstable.

In order to achieve accurate and robust trajectory tracking control, the aforementioned characteristics should be considered. To facilitate controller design, a simplified schematic model is established, as shown in Fig. 2.

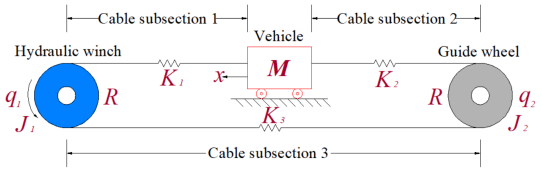

FIGURE 2. Schematic model of cable-driven underwater vehicle system.

The major forces in the cable-driven vehicle model system include: output force of hydraulic winch, cable tractions, and frictions. The entire cable is divided into three subsections, and the highly nonlinear cable dynamics of each cable subsection is expressed as a finite combination of known nonlinear functions viz. $K_{i1}\delta_i + K_{i2}\delta_i^3, i = 1, 2, 3$, where δ_i denotes the deformation of the cable subsection i, K_{i1} and K_{i2} are stiffness coefficients [10]. Frictions mainly exist between winch and cable, wheel and cable, as well as between vehicle and the ground. Since they are closely related to the running state of the system, the exact values are very difficult to measure and calculate.

According to Newton's second law of motion and law of rotation, the dynamics model of cable-driven vehicle model system is described as follows.

$$\begin{aligned}(M+\Delta M)\ddot{x} &= K_{11}(Rq_1 - x) + K_{12}(Rq_1 - x)^3 \\ &\quad - K_{21}(x - Rq_2) - K_{22}(x - Rq_2)^3 \\ &\quad - F_d - F_f - \lambda_1 \\ J_2\ddot{q}_2 &= K_{21}R(x - Rq_2) + K_{22}R(x - Rq_2)^3 \\ &\quad - K_{31}R(Rq_2 - Rq_1) - K_{32}R(Rq_2 \\ &\quad - Rq_1)^3 - F_{f2}R - \lambda_2 \\ J_1\ddot{q}_1 &= n\tau_s - K_{11}R(Rq_1 - x) - K_{12}R(Rq_1 - x)^3 \\ &\quad - K_{31}R(Rq_2 - Rq_1) - K_{32}R(Rq_2 - Rq_1)^3 \\ &\quad - F_{f1}R - \lambda_3 \end{aligned} \tag{1}$$

where M represents the mass of the vehicle, ΔM is the added mass caused by the relative motion between the vehicle and water, x is the displacement of the vehicle, R denotes the radius of hydraulic winch, and the radius of guide wheel

is the same as the radius of hydraulic winch, $q_i, i = 1, 2$ denote the angular displacements, $J_i, i = 1, 2$ denote the moments of inertia of the hydraulic winch and guide wheel, n denotes the reduction ratio of the hydraulic winch, τ_s is the output torque of hydraulic winch, F_f denotes unknown friction between the vehicle and ground, $F_d = 0.5C_d\rho A\dot{x}^2$ denotes the water resistance, where C_d is the drag force coefficient of the underwater vehicle, ρ is the water density, A is the sectional area of underwater vehicle in the direction of motion, F_{f1} and F_{f2} denote unknown frictions between wheels and the cable, $\lambda_i, i = 1, 2, 3$ represent other unknown external disturbances, including the unknown underwater disturbances, time-varying hydraulic parameters, and the leak of hydraulic systems, etc.

Due to limited output torque of hydraulic winch, there exists input saturation as

$$\tau_s = sat(u) = \begin{cases} \tau_m sign(u) & |u| \geq \tau_m \\ u & |u| < \tau_m \end{cases} \tag{2}$$

where τ_m denotes the known magnitude of the saturation limit, $sat(\cdot)$ and $sign(\cdot)$ denote the saturation function and unit sign function, respectively.

The differences between the unconstrained and constrained actuator outputs are defined as

$$\Delta u = \tau_s - u \tag{3}$$

Define the system state variables as $\mathbf{x} = \begin{bmatrix} x_1 & x_2 & x_3 & x_4 & x_5 & x_6 \end{bmatrix}^T = \begin{bmatrix} x & \dot{x} & q_2 & \dot{q}_2 & q_1 & \dot{q}_1 \end{bmatrix}^T$, the dynamics model of cable-driven vehicle model system is rewritten as

$$\begin{aligned} \dot{x}_1 &= x_2 \\ \dot{x}_2 &= x_3 + f_2 + \Delta f_2 + d_2 \\ \dot{x}_3 &= x_4 \\ \dot{x}_4 &= x_5 + f_4 + \Delta f_4 + d_4 \\ \dot{x}_5 &= x_6 \\ \dot{x}_6 &= g(u + \Delta u) + f_6 + \Delta f_6 + d_6 \end{aligned} \tag{4}$$

where $f_{(\cdot)}$ are known nonlinear functions, $\Delta f_{(\cdot)}$ denote the unknown modeling errors caused by unknown frictions, $d_{(\cdot)}$ represent the unknown compound uncertainties caused by external disturbances. Specific expressions of above functions are shown below.

$$\begin{cases} f_2 = [K_{11}(Rx_5 - x_1) + K_{12}(Rx_5 - x_1)^3 - K_{21}(x_1 - Rx_3) \\ \quad -K_{22}(x_1 - Rx_3)^3 - 0.5C_d\rho A x_2^2]/(M + \Delta M) - x_3 \\ f_4 = [K_{21}R(x_1 - Rx_3) + K_{22}R(x_1 - Rx_3)^3 \\ \quad -K_{31}R(Rx_3 - Rx_5) - K_{32}R(Rx_3 - Rx_5)^3]/J_2 - x_5 \\ f_6 = [-K_{11}R(Rx_5 - x_1) - K_{12}R(Rx_5 - x_1)^3 \\ \quad -K_{31}R(Rx_3 - Rx_5) - K_{32}R(Rx_3 - Rx_5)^3]/J_1 \\ \Delta f_2 = -F_f/(M + \Delta M) \\ \Delta f_4 = -F_{f2}R/J_2 \\ \Delta f_6 = -F_{f1}R/J_1 \\ d_2 = -\lambda_1/(M + \Delta M) \\ d_4 = -\lambda_2/J_2 \\ d_6 = -\lambda_3/J_1 \\ g = n/J_1 \end{cases}$$

B. PROBLEM FORMULATION

To improve the adaptability of our approach, the mathematical model (4) is further extended to a general nth order nonlinear uncertain system, as demonstrated below.

$$\begin{aligned} \dot{x}_1 &= x_2 \\ \dot{x}_2 &= x_3 + f_2 + \Delta f_2 + d_2 \\ &\vdots \\ \dot{x}_{2j-1} &= x_{2j} \\ \dot{x}_{2j} &= x_{2j+1} + f_{2j} + \Delta f_{2j} + d_{2j}, \quad j = 2, 3, \ldots, n/2 - 1 \\ &\vdots \\ \dot{x}_{n-1} &= x_n \\ \dot{x}_n &= g(u + \Delta u) + f_n + \Delta f_n + d_n \\ y &= x_1 \end{aligned} \tag{5}$$

where u is the control input, y is the output of system, n is order of the system, and n has to be even. $f_i, i = 2, 4, \ldots, n$ are known, smooth nonlinear functions, $\Delta f_i, i = 2, 4, \ldots, n$ are unknown modeling errors, Δu denotes the control input uncertainty caused by input saturation, $d_i, i = 2, 4, \ldots, 2n - 2$ and d_n are unknown mismatched and matched disturbances respectively.

Our objective is to develop a controller to regulate the output of high-order nonlinear system to track the desired trajectory, regardless of system nonlinearities, input saturation, modeling errors, and external disturbances. The control problem is mathematically stated as follows.

Control Problem: Given the system dynamics model (5) and desired trajectory x_{1d}, derive an effective nonlinear control law to generate the control input u, so that the tracking error $x_1 - x_{1d}$ can converge uniformly and asymptotically to zero as t goes to ∞.

To facilitate controller design, following assumptions are required.

Assumption 1: There exist positive constants $Y_0, Y_1 \ldots, Y_n$ such that the desired trajectory x_{1d} and its time derivatives satisfy $|x_{1d}| \leq Y_0$, $\left|x_{1d}^{(i)}\right| \leq Y_i, i = 1, \ldots, n$.

Assumption 2: The external disturbances $d_i, i = 2, \ldots, 2j, \ldots, n$ and their first-order time differentials have the following properties: $|d_i| \leq \bar{d}_i$, $\left|\dot{d}_i\right| \leq \bar{d}_{ci}, i = 2, \ldots, 2j, \ldots, n$, where $\bar{d}_i$ and $\bar{d}_{ci}$ represent the unknown positive upper bounds of d_i and $\dot{d}_i$, respectively.

III. ADAPTIVE TRAJECTORY TRACKING CONTROLLER DESIGN

A. CONTROL STRATEGY

As analyzed before, the discussed cable-driven vehicle model system exhibits complex high-order nonlinearities, and subjects to multi-source uncertainties and input saturation, which can severely degrade the closed-loop system performance and even make the entire system unstable. To achieve trajectory tracking control, an integrated estimation based backstepping

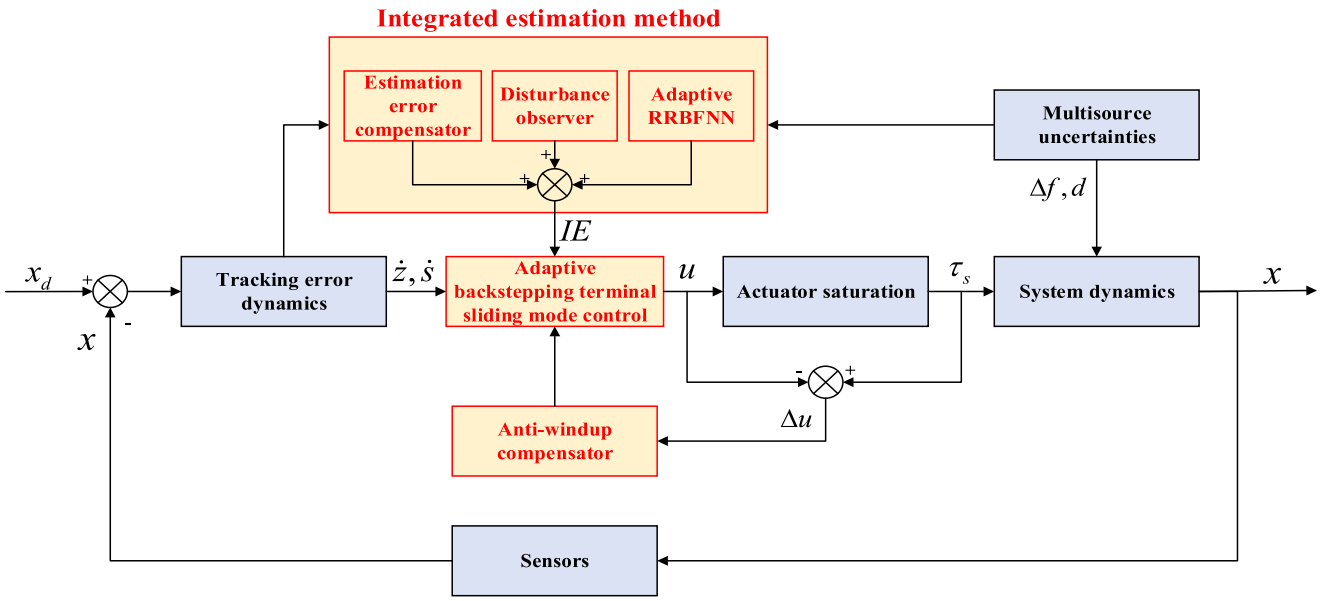

FIGURE 3. Adaptive control frame of trajectory tracking.

terminal sliding mode controller is proposed, as shown in Fig. 3.

The proposed controller mainly consists of the following three parts:

1) ***Integrated estimation:*** An integrated estimation method is proposed to handle the unknown multi-source uncertainties, utilizing RRBFNN and DO for uncertainties estimations, and adaptive robust method for estimation error compensation, which relaxes the known boundary requirement of uncertainties and helps improving the anti-jamming capability.
2) ***Adaptive backstepping terminal sliding mode control:*** Adaptive backstepping terminal sliding mode control method is chosen as the main framework of proposed controller, which helps improving system robustness and convergence efficiency. In addition, the issue of "explosion of complexity" occurred in traditional backstepping design is tackled by adaptive control method.
3) ***Anti-windup compensator:*** To reduce the influence of input saturation, an anti-windup compensator is employed.

In order to give readers a better understanding of the specific design principle, a flow chart of the proposed controller is presented in Fig. 4. It is clearly seen that the whole system is divided into n subsystems, and the virtual control law designed in the previous subsystem will act as the instruction of the next subsystem. According to different model characteristics, different control methods are employed in odd and even subsystems. In odd subsystems, after the tracking errors are calculated, Lyapunov design methods are employed to obtain the virtual control laws, whereas in even subsystems, integrated estimation methods are added to deal with the multisource uncertainties. Besides, in subsystems of orders greater than 3, adaptive methods are utilized to compensate for the issue of "explosion of complexity". In the designing process of the last subsystem, terminal sliding mode control is employed to improve system robustness and convergence efficiency, and anti-windup compensator is utilized to reduce the influence of input saturation.

Adopting the above design methods, accurate and robust trajectory tracking control of proposed cable-driven vehicle model system can be achieved. The detailed design process of the adaptive trajectory tracking controller is shown below.

B. THREE-LAYER RECURRENT RBFNN

Inspired by the work of Han *et al.* [46], a three-layer Recurrent RBFNN is utilized to estimate the unknown modeling errors, viz. Δf_i, $i = 2, 4, \ldots, n$, as shown in Fig. 5.

The principle of RRBFNN is introduced as follows:

Input Layer: There are n neurons in the input layer, and the output values of each neuron are as follows:

$$u_i(t) = x_i(t) \tag{6}$$

where $u_i(t)$ is the ith output value at time t, $i = 1, 2, \ldots, n$.

Hidden Layer: Gaussian function is adopted as the activation function, as shown below.

$$\phi_j(t) = e^{-\left\|\mathbf{h}_j(t)-\boldsymbol{\xi}_j(t)\right\| \Big/ 2\eta_j^2(t)}, \quad j = 1, 2, \ldots, m \tag{7}$$

where $\boldsymbol{\xi}_j(t)$ denotes the center vector of the jth hidden neuron at time t, $\left\|\mathbf{h}_j(t) - \boldsymbol{\xi}_j(t)\right\|$ is the Euclidean distance between $\mathbf{h}_j(t)$ and $\boldsymbol{\xi}_j(t)$, and $\eta_j(t)$ is the radius or width of the jth hidden neuron at time t. $\mathbf{h}_j(t)$ is the input vector of the jth hidden neuron described by

$$\mathbf{h}_j(t) = \left[u_1(t), u_2(t), \ldots, u_n(t), v_j(t) \cdot y(t-1)\right]^T \tag{8}$$

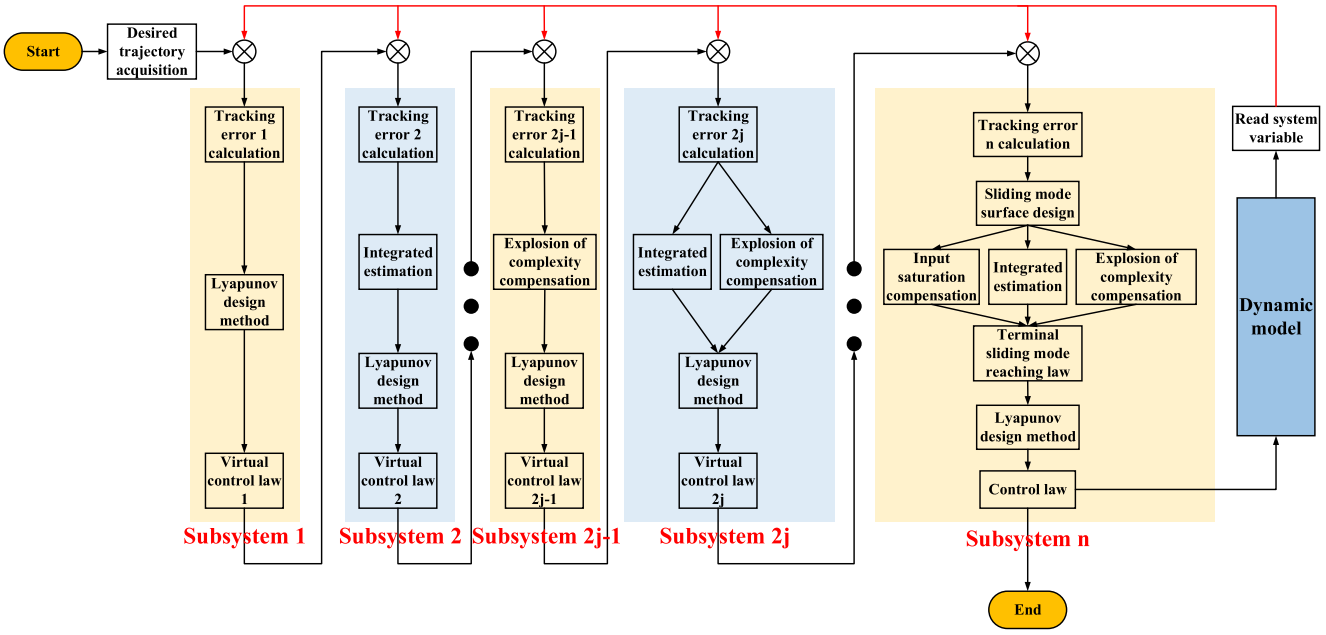

FIGURE 4. Flow chart of the trajectory tracking controller design.

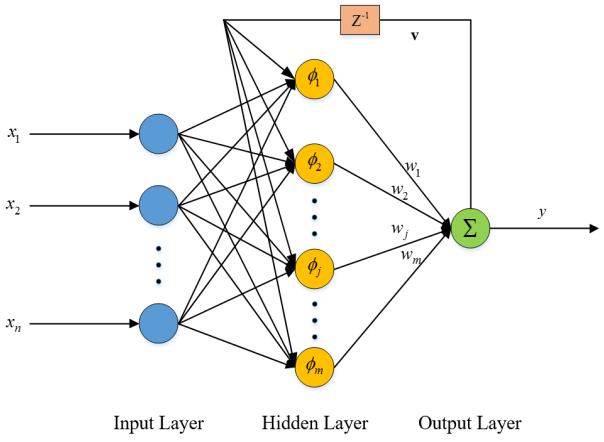

FIGURE 5. Structure of recurrent RBFNN.

where $y(t-1)$ is the output value of output layer at time t-1, $v_j(t)$ denotes the connection weight from output layer to the jth hidden neuron at time t.

Output Layer: There is only one node in this layer, and the output is as follows:

$$y(t) = \mathbf{W}^T(t)\mathbf{\Phi}(t) = \sum_{j=1}^{m} w_j(t)\phi_j(t) \tag{9}$$

where $\mathbf{W}(t) = [w_1(t), w_2(t), \ldots, w_m(t)]^T$ is the connection weight matrix between the hidden layer and output layer, $\mathbf{\Phi}(t) = [\phi_1(t), \phi_2(t), \ldots, \phi_m(t)]^T$ is the output vector matrix of the hidden layer.

Estimation Error Analysis: If RRBFNN is utilized to approximate an unknown and continuous function $f(x)$, the estimation value can be expressed as

$$\hat{f}(x) = \hat{\mathbf{W}}^T \mathbf{\Phi}(x, \xi) \tag{10}$$

And the actual function can be rewritten as

$$f(x) = \hat{\mathbf{W}}^T \mathbf{\Phi}(x, \xi) + \varepsilon(x) \tag{11}$$

where $\varepsilon(x)$ is the approximation error which satisfy $|\varepsilon(x)| \leq \bar{\varepsilon}$ with $\bar{\varepsilon} > 0$.

It has been proved that RBFNN can smoothly approximate any unknown and continuous function $f(x)$ with arbitrary precision [47]. Therefore, $f(x)$ can be rewritten as

$$f(x) = \mathbf{W}^{*T} \mathbf{\Phi}(x, \xi) + \varepsilon^*(x) \tag{12}$$

where $\mathbf{W}^{*T}$ is the optimal weight, $\varepsilon^*(x)$ denotes the optimal approximation error.

The optimal weight of RRBFNN can be given by

$$\mathbf{W}^{*T} = \arg \min_{\hat{\mathbf{W}}^T \in R} \left\{ \sup \left| f(x) - \hat{\mathbf{W}}^T \phi(x, \xi) \right| \right\} \tag{13}$$

Using the optimal weight value yields

$$\sup \left| f(x) - \hat{f}(x) \right| = \left| \varepsilon^*(x) \right| \leq |\varepsilon(x)| \leq \bar{\varepsilon} \tag{14}$$

C. CONTROLLER DESIGN

During the designing procedure, following tracking error variables are defined:

$$z_i = x_i - x_{id}, \quad i = 1, 2, \ldots, n \tag{15}$$

where x_{1d} denotes the given ideal trajectory, x_{id}, $i = 2, \ldots, n$ are the designed virtual control laws.

Step 1: The tracking error dynamics of subsystem 1 is

$$\dot{z}_1 = \dot{x}_1 - \dot{x}_{1d} = x_2 - \dot{x}_{1d} \tag{16}$$

The virtual control law x_{2d} is designed as

$$x_{2d} = \dot{x}_{1d} - k_1 z_1 \tag{17}$$

where $k_1 > 0$.

Consider the following Lyapunov function candidate

$$V_1 = \frac{1}{2} z_1^2 \tag{18}$$

Utilizing the virtual control law, the time derivative of V_1 is derived as

$$\begin{aligned} \dot{V}_1 &= z_1 \dot{z}_1 \\ &= z_1 z_2 - k_1 z_1^2 \\ &\le \frac{1}{2\sigma 10} z_1^2 + \frac{\sigma 10}{2} z_2^2 - k_1 z_1^2 \\ &= -(k_1 - \frac{1}{2\sigma 10}) z_1^2 + \frac{\sigma 10}{2} z_2^2 \end{aligned} \tag{19}$$

where $\sigma 10$ is designed positive constant, and the design parameters are chosen to satisfy the condition $k_1 - \frac{1}{2\sigma 10} > 0$.

It can be concluded from (19) that $\dot{V}_1 < 0$ as long as $z_1^2 > \frac{\sigma 10}{2} z_2^2 \Big/ (k_1 - \frac{1}{2\sigma 10})$. Consequently, the decrease of V_1 will drive z_1 into $|z_1| \le \sqrt{\frac{\sigma 10}{2} z_2^2 \Big/ (k_1 - \frac{1}{2\sigma 10})}$.

Remark 1: Apparently, if z_2 is converged, the state tracking error z_1 will be bounded. Hence, it is proved that under the proposed virtual control input x_{2d}, the tracking error z_1 is converging and bounded to a specified compact set Ω_{z1} which can be defined by $\Omega_{z1} = \left\{ z_1 \in R \left| |z_1| \le \sqrt{\frac{\sigma 10}{2} z_2^2 \Big/ (k_1 - \frac{1}{2\sigma 10})} \right. \right\}$.

Step 2: Utilizing optimal RRBFNN, the time derivative of state variable x_2 is rewritten as

$$\dot{x}_2 = x_3 + f_2 + \mathbf{W}_2^{*T} \mathbf{\Phi}_2 + \varepsilon_2^* + d_2 \tag{20}$$

where $\mathbf{W}_2^{*T}$ is the optimal weight matrix, $\mathbf{\Phi}_2$ is the radial basis function, ε_2^* is the smallest approximation error.

The tracking error dynamics of subsystem 2 is derived as

$$\dot{z}_2 = x_3 + f_2 + \mathbf{W}_2^{*T} \mathbf{\Phi}_2 + \varepsilon_2^* + d_2 - \dot{x}_{2d} \tag{21}$$

where $\dot{x}_{2d} = \ddot{x}_{1d} - k_1 \dot{z}_1 = \ddot{x}_{1d} - k_1 \dot{x}_1 + k_1 \dot{x}_{1d}$.

To estimate and compensate for the unknown modeling error Δf_2 and external disturbance d_2, following integrated estimation function is utilized:

$$IE_2 = \hat{\mathbf{W}}_2^T \mathbf{\Phi}_2 + \hat{\varepsilon}_2 + \hat{d}_2 + \frac{\hat{\delta}_2^2 z_2}{\left| \hat{\delta}_2 z_2 \right| + c_2 e^{-a_2 t}} \tag{22}$$

where $\hat{\mathbf{W}}_2^T \mathbf{\Phi}_2$ is the RRBFNN utilized to approximate Δf_2, and $\hat{\mathbf{W}}_2^T$ is the designed weight matrix, $\hat{\varepsilon}_2$ is the estimation of ε_2^*, $\hat{d}_2$ is the disturbance observer utilized to estimate d_2, $\frac{\hat{\delta}_2^2 z_2}{\left| \hat{\delta}_2 z_2 \right| + c_2 e^{-a_2 t}}$ is an adaptive robust term designed to compensate for the observation error $\tilde{d}_2$, and $\hat{\delta}_2$ is the estimation of $\tilde{d}_2$, $a_2 > 0$, $c_2 > 0$.

The disturbance observer utilized in (22) is designed as

$$\begin{aligned} \hat{d}_2 &= \varphi_2 + \lambda_2 x_2 \\ \dot{\varphi}_2 &= -\lambda_2 (x_3 + f_2 + \hat{\mathbf{W}}_2^T \mathbf{\Phi}_2 + \hat{d}_2) \end{aligned} \tag{23}$$

where φ_2 is the auxiliary variable, and $\lambda_2 > 0$ is the designed parameter.

Based on (20) and (23), one can obtain

$$\begin{aligned} \dot{\hat{d}}_2 &= \dot{\varphi}_2 + \lambda_2 \dot{x}_2 \\ &= -\lambda_2 (x_3 + f_2 + \hat{\mathbf{W}}_2^T \mathbf{\Phi}_2 + \hat{d}_2) \\ &\quad + \lambda_2 (x_3 + f_2 + \mathbf{W}_2^{*T} \mathbf{\Phi}_2 + \varepsilon_2^* + d_2) \\ &= \lambda_2 (\tilde{\mathbf{W}}_2^T \mathbf{\Phi}_2 + \varepsilon_2^* + \tilde{d}_2) \end{aligned} \tag{24}$$

where $\tilde{\mathbf{W}}_2^T = \mathbf{W}_2^{*T} - \hat{\mathbf{W}}_2^T$, $\tilde{d}_2 = d_2 - \hat{d}_2$.

The parameter updating laws of IE_2 are designed as

$$\begin{aligned} \dot{\hat{\mathbf{W}}}_2 &= r_{21} z_2 \mathbf{\Phi}_2 \\ \dot{\hat{\varepsilon}}_2 &= r_{23} z_2 \\ \dot{\hat{\delta}}_2 &= r_{24} z_2 \end{aligned} \tag{25}$$

where $r_{21} > 0$, $r_{23} > 0$, $r_{24} > 0$.

The virtual control law x_{3d} is designed as

$$x_{3d} = -f_2 - IE_2 + \dot{x}_{2d} - k_2 z_2 \tag{26}$$

where $k_2 > 0$ is the designed parameter.

Theorem 1: Utilizing integrated estimation function (22), parameter updating law (25), and virtual control law (26), tracking error z_2 can converge to a specified compact set.

Proof 1: Consider the Lyapunov function candidate as

$$\begin{aligned} V_2 = \frac{1}{2} z_2^2 + \frac{1}{2 r_{21}} \tilde{\mathbf{W}}_2^T \tilde{\mathbf{W}}_2 + \frac{1}{2 r_{22}} \tilde{d}_2^2 + \frac{1}{2 r_{23}} \tilde{\varepsilon}_2^2 \\ + \frac{1}{2 r_{24}} \tilde{\delta}_2^2 + \frac{c_2}{a_2} e^{-a_2 t} \end{aligned} \tag{27}$$

where $\tilde{\varepsilon}_2 = \varepsilon_2^* - \hat{\varepsilon}_2$, $\tilde{\delta}_2 = \tilde{d}_2 - \hat{\delta}_2$, $r_{22} > 0$.

The time derivative of V_2 is derived as

$$\begin{aligned} \dot{V}_2 &= z_2 \dot{z}_2 + \frac{1}{r_{21}} \tilde{\mathbf{W}}_2^T \dot{\tilde{\mathbf{W}}}_2 \\ &\quad + \frac{1}{r_{22}} \tilde{d}_2 \dot{\tilde{d}}_2 + \frac{1}{r_{23}} \tilde{\varepsilon}_2 \dot{\tilde{\varepsilon}}_2 + \frac{1}{r_{24}} \tilde{\delta}_2 \dot{\tilde{\delta}}_2 - c_2 e^{-a_2 t} \\ &= z_2 (z_3 + x_{3d} + f_2 + \mathbf{W}_2^{*T} \mathbf{\Phi}_2 + \varepsilon_2^* + d_2 - \dot{x}_{2d}) \\ &\quad + \frac{1}{r_{21}} \tilde{\mathbf{W}}_2^T (\dot{\mathbf{W}}_2^* - \dot{\hat{\mathbf{W}}}_2) + \frac{1}{r_{22}} \tilde{d}_2 (\dot{d}_2 - \dot{\hat{d}}_2) \\ &\quad + \frac{1}{r_{23}} \tilde{\varepsilon}_2 (\dot{\varepsilon}_2^* - \dot{\hat{\varepsilon}}_2) + \frac{1}{r_{24}} \tilde{\delta}_2 (\dot{\tilde{d}}_2 - \dot{\hat{\delta}}_2) - c_2 e^{-a_2 t} \end{aligned} \tag{28}$$

Substituting (22-26) into (28), one can obtain

$$\begin{aligned} \dot{V}_2 = z_2 z_3 - k_2 z_2^2 + \frac{1}{r_{22}} \tilde{d}_2 \dot{d}_2 - \frac{\lambda_2}{r_{22}} \tilde{d}_2 (\tilde{\mathbf{W}}_2^T \mathbf{\Phi}_2 + \varepsilon_2^* + \tilde{d}_2) \\ + \frac{1}{r_{24}} \tilde{\delta}_2 \dot{\tilde{d}}_2 + z_2 (\tilde{d}_2 - \tilde{\delta}_2) - c_2 e^{-a_2 t} - \frac{\hat{\delta}_2^2 z_2^2}{\left| \hat{\delta}_2 z_2 \right| + c_2 e^{-a_2 t}} \end{aligned}$$

$$\leq z_2 z_3 - k_2 z_2^2 + \frac{1}{r_{22}}\tilde{d}_2\dot{d}_2 - \frac{\lambda_2}{r_{22}}\tilde{d}_2(\tilde{\mathbf{W}}_2^T\boldsymbol{\Phi}_2 + \varepsilon_2^* + \tilde{d}_2) + \frac{1}{r_{24}}\tilde{\delta}_2\dot{\tilde{d}}_2 + \left|\hat{\delta}_2 z_2\right| - c_2 e^{-a_2 t} - \frac{\hat{\delta}_2^2 z_2^2}{\left|\hat{\delta}_2 z_2\right| + c_2 e^{-a_2 t}}$$
$$\leq z_2 z_3 - k_2 z_2^2 + \frac{1}{r_{22}}\tilde{d}_2\dot{d}_2 - \frac{\lambda_2}{r_{22}}\tilde{d}_2\tilde{\mathbf{W}}_2^T\boldsymbol{\Phi}_2 - \frac{\lambda_2}{r_{22}}\tilde{d}_2\varepsilon_2^* - \frac{\lambda_2}{r_{22}}\tilde{d}_2^2 + \frac{1}{r_{24}}\tilde{\delta}_2\dot{\tilde{d}}_2 \tag{29}$$

Considering the constraints $|\phi_2| \leq 1$, $\left|\dot{d}_2\right| \leq \bar{d}_{c2}$, and $\left|\varepsilon_2^*\right| \leq \bar{\varepsilon}_2$, the time derivative of V_2 can be further derived as

$$\dot{V}_2 \leq z_2 z_3 - k_2 z_2^2 + \frac{1}{r_{22}}\left|\tilde{d}_2\right|\left|\bar{d}_{c2}\right| + \frac{\lambda_2}{r_{22}}\left|\tilde{d}_2\right|\left|\tilde{\mathbf{W}}_2^T\right| + \frac{\lambda_2}{r_{22}}\left|\tilde{d}_2\right||\bar{\varepsilon}_2| - \frac{\lambda_2}{r_{22}}\tilde{d}_2^2 + \frac{1}{r_{24}}\left|\tilde{\delta}_2\right|\left|\dot{\tilde{d}}_2\right|$$
$$\leq z_2 z_3 - k_2 z_2^2 + \frac{1}{2\sigma_{21}}\frac{1}{r_{22}}\tilde{d}_2^2 + \frac{\sigma_{21}}{2}\frac{1}{r_{22}}\bar{d}_{c2}^2 + \frac{1}{2\sigma_{22}}\frac{\lambda_2}{r_{22}}\tilde{d}_2^2 + \frac{\sigma_{22}}{2}\frac{\lambda_2}{r_{22}}\tilde{\mathbf{W}}_2^T\tilde{\mathbf{W}}_2 + \frac{1}{2\sigma_{23}}\frac{\lambda_2}{r_{22}}\tilde{d}_2^2 + \frac{\sigma_{23}}{2}\frac{\lambda_2}{r_{22}}\bar{\varepsilon}_2^2 + \frac{1}{2\sigma_{24}}\frac{1}{r_{24}}\tilde{\delta}_2^2 + \frac{\sigma_{24}}{2}\frac{1}{r_{24}}\dot{\tilde{d}}_2^2 - \frac{\lambda_2}{r_{22}}\tilde{d}_2^2$$
$$\leq -(k_2 - \frac{1}{2\sigma_{20}})z_2^2 + \frac{\sigma_{20}}{2}z_3^2 + \frac{\sigma_{22}\lambda_2}{2r_{22}}\tilde{\mathbf{W}}_2^T\tilde{\mathbf{W}}_2 + \frac{1}{2\sigma_{24}r_{24}}\tilde{\delta}_2^2 + \frac{\sigma_{24}}{2}\frac{1}{r_{24}}\dot{\tilde{d}}_2^2 + (\frac{\sigma_{21}}{2r_{22}}\bar{d}_{c2}^2 + \frac{\sigma_{23}\lambda_2}{2r_{22}}\bar{\varepsilon}_2^2) \tag{30}$$

where σ_{2i}, $i = 0, 1, 2, 3, 4$ are designed positive constants, and the parameters can be chosen to guarantee $k_2 - \frac{1}{2\sigma_{20}} > 0$ and $\frac{\lambda_2}{r_{22}} - \frac{1}{2\sigma_{21}r_{22}} - \frac{\lambda_2}{2\sigma_{22}r_{22}} - \frac{\lambda_2}{2\sigma_{23}r_{22}} > 0$.

Define

$$\Gamma_2 = \frac{\sigma_{22}\lambda_2}{2r_{22}}\tilde{\mathbf{W}}_2^T\tilde{\mathbf{W}}_2 + \frac{1}{2\sigma_{24}r_{24}}\tilde{\delta}_2^2 + \frac{\sigma_{24}}{2}\frac{1}{r_{24}}\dot{\tilde{d}}_2^2 + (\frac{\sigma_{21}}{2r_{22}}\bar{d}_{c2}^2 + \frac{\sigma_{23}\lambda_2}{2r_{22}}\bar{\varepsilon}_2^2),$$

Then (30) is rewritten as

$$\dot{V}_2 \leq -(k_2 - \frac{1}{2\sigma_{20}})z_2^2 + \frac{\sigma_{20}}{2}z_3^2 + \Gamma_2 \tag{31}$$

Remark 2: Assume $\tilde{\mathbf{W}}_2$, $\tilde{\delta}_2$, and $\dot{\tilde{d}}_2$ are bounded, and then Γ_2 will be bounded. Moreover, if z_3 is bounded, the state tracking error z_2 will be converged. Hence, it is proved that under the proposed virtual control input x_{3d}, the state tracking error z_2 is converging and bounded to a specified compact set Ω_{z2} defined by $\Omega_{z2} = \left\{z_2 \in R \middle| |z_2| \leq \sqrt{(\frac{\sigma_{20}}{2}z_3^2 + \Gamma_2)\Big/(k_2 - \frac{1}{2\sigma_{20}})}\right\}$.

Step 2j−1 (j = 2, …, n/2−1): The time derivative of z_{2j-1} is

$$\dot{z}_{2j-1} = \dot{x}_{2j-1} - \dot{x}_{(2j-1)d} = x_{2j} - \dot{x}_{(2j-1)d} \tag{32}$$

The original virtual control law $x_{(2j)d}$ should be $x_{(2j)d} = \dot{x}_{(2j-1)d} - k_{2j-1}z_{2j-1}$. However, $\dot{x}_{(2j-1)d}$ is too complex to calculate. Take $\dot{x}_{3d}$ as an example, according to (26), $\dot{x}_{3d}$ is calculated as

$$\dot{x}_{3d} = -\frac{\partial f_2}{\partial x_1}\dot{x}_1 - \frac{\partial f_2}{\partial x_2}\dot{x}_2 - \frac{\partial f_2}{\partial x_3}\dot{x}_3 - \frac{\partial f_2}{\partial x_5}\dot{x}_5 - \dot{\hat{\mathbf{W}}}_2^T\boldsymbol{\Phi}_2 - \dot{\hat{\varepsilon}}_2 - \dot{\hat{d}}_2 + \ddot{x}_{2d} - k_2\dot{z}_2 - \partial(\frac{\hat{\delta}_2^2 z_2}{\left|\hat{\delta}_2 z_2\right| + c_2 e^{-a_2 t}})\dot{z}_2 \Big/ \partial z_2 \tag{33}$$

Apparently, the calculation of $\dot{x}_{3d}$ will bring considerable computational burdens. As the backstepping procedure goes, the situation will be more and more serious, which may eventually cause the "explosion of complexity" problem. Inspired by Wu *et al.* [14], an adaptive method is utilized to tackle this problem. To facilitate the remaining design procedure, following assumption is required.

Assumption 3: There exist positive constants χ_i such that the time-derivatives of virtual control laws x_{id}, $i = 3, \ldots, n$ satisfy $|\dot{x}_{id}| < \chi_i$, $i = 3, \ldots, n$.

To avoid "explosion of complexity" problem, the new virtual control law $x_{(2j)d}$ is designed as

$$x_{(2j)d} = -\frac{\hat{p}_{2j-1}z_{2j-1}}{2\varsigma_{2j-1}^2} - k_{2j-1}z_{2j-1} \tag{34}$$

where $k_{2j-1} > 0$, $\varsigma_{2j-1} > 0$, $\hat{p}_{2j-1}$ is the adaptive term with the updating law as follows.

$$\dot{\hat{p}}_{2j-1} = \frac{\beta_{2j-1}z_{2j-1}^2}{2\varsigma_{2j-1}^2} - \alpha_{2j-1}\hat{p}_{2j-1},\ \alpha_{2j-1} > 0,\ \beta_{2j-1} > 0 \tag{35}$$

Theorem 2: Utilizing virtual control law (34) and parameter updating law (35), the state tracking error z_{2j-1} is guaranteed to converge to a specified compact set.

Proof 2: Consider the following Lyapunov function candidate

$$V_{2j-1} = \frac{1}{2}z_{2j-1}^2 + \frac{1}{2\beta_{2j-1}}(\chi_{2j-1}^2 - \hat{p}_{2j-1})^2 \tag{36}$$

The time derivative of V_{2j-1} is derived as

$$\dot{V}_{2j-1} = z_{2j-1}z_{2j} - k_{2j-1}z_{2j-1}^2 - z_{2j-1}\dot{x}_{(2j-1)d} - \frac{\chi_{2j-1}^2 z_{2j-1}^2}{2\varsigma_{2j-1}^2} + \frac{\alpha_{2j-1}\hat{p}_{2j-1}}{\beta_{2j-1}}\chi_{2j-1}^2 - \frac{\alpha_{2j-1}}{\beta_{2j-1}}\hat{p}_{2j-1}^2$$
$$\leq z_{2j-1}z_{2j} - k_{2j-1}z_{2j-1}^2 + \frac{1}{2\sigma_{(2j-1)1}}z_{2j-1}^2 + \frac{\sigma_{(2j-1)1}}{2}\chi_{2j-1}^2 - \frac{\chi_{2j-1}^2 z_{2j-1}^2}{2\varsigma_{2j-1}^2} + \frac{\alpha_{2j-1}\hat{p}_{2j-1}}{\beta_{2j-1}}\chi_{2j-1}^2 - \frac{\alpha_{2j-1}}{\beta_{2j-1}}\hat{p}_{2j-1}^2$$
$$\leq z_{2j-1}z_{2j} - (k_{2j-1} - \frac{1}{2\sigma_{(2j-1)1}} - \frac{\chi_{2j-1}^2}{2\varsigma_{2j-1}^2})z_{2j-1}^2 + \frac{\sigma_{(2j-1)1}}{2}\chi_{2j-1}^2 + \frac{\alpha_{2j-1}}{4\beta_{2j-1}}\chi_{2j-1}^4$$
$$\leq -(k_{2j-1} - \frac{1}{2\sigma_{(2j-1)0}} - \frac{1}{2\sigma_{(2j-1)1}} - \frac{\chi_{2j-1}^2}{2\varsigma_{2j-1}^2})z_{2j-1}^2 + \frac{1}{2\sigma_{(2j-1)0}}z_{2j}^2 + \frac{\sigma_{(2j-1)1}}{2}\chi_{2j-1}^2 + \frac{\alpha_{2j-1}}{4\beta_{2j-1}}\chi_{2j-1}^4 \tag{37}$$

where $\sigma_{(2j-1)0}$ and $\sigma_{(2j-1)1}$ are designed positive constants, and the design parameters are chosen to satisfy

$$k_{2j-1} - \frac{1}{2\sigma_{(2j-1)0}} - \frac{1}{2\sigma_{(2j-1)1}} - \frac{\chi_{2j-1}^2}{2\varsigma_{2j-1}^2} > 0.$$

Define $\Gamma_{2j-1} = \frac{\sigma_{(2j-1)1}}{2}\chi_{2j-1}^2 + \frac{\alpha_{2j-1}}{4\beta_{2j-1}}\chi_{2j-1}^4$, then (37) is rewritten as

$$\dot{V}_{2j-1} \le -(k_{2j-1} - \frac{1}{2\sigma_{(2j-1)0}} - \frac{1}{2\sigma_{(2j-1)1}} - \frac{\chi_{2j-1}^2}{2\varsigma_{2j-1}^2})z_{2j-1}^2 + \frac{1}{2\sigma_{(2j-1)0}}z_{2j}^2 + \Gamma_{2j-1} \quad (38)$$

Remark 3: According to Assumption 3, Γ_{2j-1} is bounded. Moreover, if z_{2j} is bounded, the state tracking error z_{2j-1} will be converged. Hence, it is proved that under the proposed virtual control input $x_{(2j)d}$, z_{2j-1} is converging and bounded to a specified compact set

$$\Omega_{z(2j-1)} = \left\{ z_{2j-1} \in R \left| |z_{2j-1}| \le \sqrt{\frac{\frac{1}{2\sigma_{(2j-1)0}}z_{2j}^2 + \Gamma_{2j-1}}{k_{2j-1} - \frac{1}{2\sigma_{(2j-1)0}} - \frac{1}{2\sigma_{(2j-1)1}} - \frac{\chi_{2j-1}^2}{2\varsigma_{2j-1}^2}}} \right. \right\}.$$

Step 2j (j = 2, …, n/2−1): The dynamics model of subsystem $2j$ also contains unknown modeling error and external disturbance. To compensate for the effects of model uncertainties, integrated estimation function is also utilized here:

$$IE_{2j} = \hat{\mathbf{W}}_{2j}^T\mathbf{\Phi}_{2j} + \hat{\varepsilon}_{2j} + \hat{d}_{2j} + \frac{\hat{\delta}_{2j}^2 z_{2j}}{\left|\hat{\delta}_{2j}z_{2j}\right| + c_{2j}e^{-a_{2j}t}} \quad (39)$$

where $\hat{\mathbf{W}}_{2j}^T\mathbf{\Phi}_{2j}$ is utilized to approximate Δf_{2j}, and $\hat{\mathbf{W}}_{2j}^T$ is the designed weight matrix, $\hat{\varepsilon}_{2j}$ is the estimation of ε_{2j}^*, $\hat{d}_{2j}$ is the disturbance observer utilized to estimate d_{2j}, $\frac{\hat{\delta}_{2j}^2 z_{2j}}{\left|\hat{\delta}_{2j}z_{2j}\right| + c_{2j}e^{-a_{2j}t}}$ is an adaptive robust term designed to compensate for the observation error $\tilde{d}_{2j}$, and $\hat{\delta}_{2j}$ is the estimation of $\tilde{d}_{2j}$, $a_{2j} > 0$, $c_{2j} > 0$.

Similar with (23), following disturbance observer is utilized:

$$\begin{aligned} \hat{d}_{2j} &= \varphi_{2j} + \lambda_{2j}x_{2j} \\ \dot{\varphi}_{2j} &= -\lambda_{2j}(x_{2j+1} + f_{2j} + \hat{\mathbf{W}}_{2j}^T\mathbf{\Phi}_{2j} + \hat{d}_{2j}) \end{aligned} \quad (40)$$

where φ_{2j} is the auxiliary variable, and $\lambda_{2j} > 0$ is the designed parameter.

The virtual control law $x_{(2j+1)d}$ is designed as

$$x_{(2j+1)d} = -f_{2j} - IE_{2j} - k_{2j}z_{2j} - \frac{\hat{p}_{2j}z_{2j}}{2\varsigma_{2j}^2} \quad (41)$$

where $\hat{p}_{2j}$ is the adaptive term designed for $\dot{x}_{(2j)d}$, $k_{2j} > 0$, $\varsigma_{2j} > 0$.

The parameter updating laws are designed as

$$\begin{aligned} \dot{\hat{\mathbf{W}}}_{2j} &= r_{(2j)1}z_{2j}\mathbf{\Phi}_{2j} \\ \dot{\hat{\varepsilon}}_{2j} &= r_{(2j)3}z_{2j} \\ \dot{\hat{\delta}}_{2j} &= r_{(2j)4}z_{2j} \\ \dot{\hat{p}}_{2j} &= \frac{\beta_{2j}z_{2j}^2}{2\varsigma_{2j}^2} - \alpha_{2j}\hat{p}_{2j}, \quad \alpha_{2j} > 0,\ \beta_{2j} > 0 \end{aligned} \quad (42)$$

Consider the following Lyapunov function candidate

$$V_{2j} = \frac{1}{2}z_{2j}^2 + \frac{1}{2r_{(2j)1}}\tilde{\mathbf{W}}_{2j}^T\tilde{\mathbf{W}}_{2j} + \frac{1}{2r_{(2j)2}}\tilde{d}_{2j}^2 + \frac{1}{2r_{(2j)3}}\tilde{\varepsilon}_{2j}^2 + \frac{1}{2r_{(2j)4}}\tilde{\delta}_{2j}^2 + \frac{1}{2\beta_{2j}}(\chi_{2j}^2 - \hat{p}_{2j})^2 + \frac{c_{2j}}{a_{2j}}e^{-a_{2j}t} \quad (43)$$

where $\tilde{\varepsilon}_{2j} = \varepsilon_{2j}^* - \hat{\varepsilon}_{2j}$, $\tilde{\delta}_{2j} = \tilde{d}_{2j} - \hat{\delta}_{2j}$, $r_{(2j)1} > 0$, $r_{(2j)2} > 0$, $r_{(2j)3} > 0$, $r_{(2j)4} > 0$.

The time derivative of V_{2j} is derived as

$$\begin{aligned} \dot{V}_{2j} = {} & z_{2j}(z_{2j+1} + x_{(2j+1)d} + f_{2j} + \mathbf{W}_{2j}^{*T}\mathbf{\Phi}_{2j} + \varepsilon_{2j}^* + d_{2j} - \dot{x}_{(2j)d}) \\ & + \frac{1}{r_{(2j)1}}\tilde{\mathbf{W}}_{2j}^T(\dot{\mathbf{W}}_{2j}^* - \dot{\hat{\mathbf{W}}}_{2j}) + \frac{1}{r_{(2j)2}}\tilde{d}_{2j}(\dot{d}_{2j} - \dot{\hat{d}}_{2j}) \\ & + \frac{1}{r_{(2j)3}}\tilde{\varepsilon}_{2j}(\dot{\varepsilon}_{2j}^* - \dot{\hat{\varepsilon}}_{2j}) + \frac{1}{r_{(2j)4}}\tilde{\delta}_{2j}(\dot{\tilde{d}}_{2j} - \dot{\hat{\delta}}_{2j}) \\ & - c_{2j}e^{-a_{2j}t} - \frac{1}{\beta_{2j}}(\chi_{2j}^2 - \hat{p}_{2j})(\frac{\beta_{2j}z_{2j}^2}{2\varsigma_{2j}^2} - \alpha_{2j}\hat{p}_{2j}) \end{aligned} \quad (44)$$

Combining the deriving methods presented in Theorem 1 and Theorem 2, one can obtain

$$\begin{aligned} \dot{V}_{2j} \le {} & z_{2j}z_{2j+1} - (k_{2j} - \frac{1}{2\sigma_{(2j)5}} - \frac{\chi_{2j}^2}{2\varsigma_{2j}^2})z_{2j}^2 - (\frac{\lambda_{2j}}{r_{(2j)2}} - \frac{1}{2\sigma_{(2j)1}r_{(2j)2}} \\ & - \frac{\lambda_{2j}}{2\sigma_{(2j)2}r_{(2j)2}} - \frac{\lambda_{2j}}{2\sigma_{(2j)3}r_{(2j)2}})\tilde{d}_{2j}^2 + \frac{\sigma_{(2j)2}\lambda_{2j}}{2r_{(2j)2}}\tilde{\mathbf{W}}_{2j}^T\tilde{\mathbf{W}}_{2j} \\ & + \frac{1}{2\sigma_{(2j)4}r_{(2j)4}}\tilde{\delta}_{2j}^2 + \frac{\sigma_{(2j)4}}{2r_{(2j)4}}\dot{\tilde{d}}_{2j}^2 + \frac{\sigma_{(2j)1}}{2r_{(2j)2}}\bar{d}_{c2j}^2 \\ & + \frac{\sigma_{(2j)3}\lambda_{2j}}{2r_{(2j)2}}\bar{\varepsilon}_{2j}^2 + (\frac{\sigma_{(2j)5}}{2} + \frac{\alpha_{2j}\hat{p}_{2j}}{\beta_{2j}})\chi_{2j}^2 - \frac{\alpha_{2j}}{\beta_{2j}}\hat{p}_{2j}^2 \\ \le {} & -(k_{2j} - \frac{1}{2\sigma_{(2j)0}} - \frac{1}{2\sigma_{(2j)5}} - \frac{\chi_{2j}^2}{2\varsigma_{2j}^2})z_{2j}^2 + \frac{\sigma_{(2j)0}}{2}z_{2j+1}^2 \\ & + \frac{\sigma_{(2j)2}\lambda_{2j}}{2r_{(2j)2}}\tilde{\mathbf{W}}_{2j}^T\tilde{\mathbf{W}}_{2j} + \frac{1}{2\sigma_{(2j)4}r_{(2j)4}}\tilde{\delta}_{2j}^2 + \frac{\sigma_{(2j)4}}{2r_{(2j)4}}\dot{\tilde{d}}_{2j}^2 \\ & + \frac{\sigma_{(2j)1}}{2r_{(2j)2}}\bar{d}_{c2j}^2 + \frac{\sigma_{(2j)3}\lambda_{2j}}{2r_{(2j)2}}\bar{\varepsilon}_{2j}^2 + \frac{\sigma_{(2j)5}}{2}\chi_{2j}^2 + \frac{\alpha_{2j}}{4\beta_{2j}}\chi_{2j}^4 \end{aligned} \quad (45)$$

where $\sigma_{(2j)i}$, $i = 0, 1, 2, 3, 4, 5$ are designed positive constants, and the parameters are chosen to guarantee the condition that $k_{2j} - \frac{1}{2\sigma_{(2j)0}} - \frac{1}{2\sigma_{(2j)5}} - \frac{\chi_{2j}^2}{2\varsigma_{2j}^2} > 0$ and $\frac{\lambda_{2j}}{r_{(2j)2}} - \frac{1}{2\sigma_{(2j)2}r_{(2j)2}} - \frac{\lambda_{2j}}{2\sigma_{(2j)2}r_{(2j)2}} - \frac{\lambda_{2j}}{2\sigma_{(2j)3}r_{(2j)2}} \ge 0$.

Auxiliary variable Γ_{2j} is defined as follows.

$$\Gamma_{2j} = \frac{\sigma_{(2j)2}\lambda_{2j}}{2r_{(2j)2}}\tilde{\mathbf{W}}_{2j}^T\tilde{\mathbf{W}}_{2j} + \frac{1}{2\sigma_{(2j)4}r_{(2j)4}}\tilde{\delta}_{2j}^2 + \frac{\sigma_{(2j)4}}{2r_{(2j)4}}\dot{\tilde{d}}_{2j}^2 + \frac{\sigma_{(2j)1}}{2r_{(2j)2}}\bar{d}_{c2j}^2 + \frac{\sigma_{(2j)3}\lambda_{2j}}{2r_{(2j)2}}\bar{\varepsilon}_{2j}^2 + \frac{\sigma_{(2j)5}}{2}\chi_{2j}^2 + \frac{\alpha_{2j}}{4\beta_{2j}}\chi_{2j}^4$$

Then (45) is rewritten as

$$\dot{V}_{2j} \le -(k_{2j} - \frac{1}{2\sigma_{(2j)0}} - \frac{1}{2\sigma_{(2j)5}} - \frac{\chi_{2j}^2}{2\varsigma_{2j}^2})z_{2j}^2 + \frac{\sigma_{(2j)0}}{2}z_{2j+1}^2 + \Gamma_{2j} \tag{46}$$

Remark 4: Assume $\tilde{\mathbf{W}}_{2j}$, $\tilde{\delta}_{2j}$, and $\dot{\tilde{d}}_{2j}$ are bounded, and then Γ_{2j} will be bounded. Moreover, if z_{2j+1} is bounded, the state tracking error z_{2j} will be converged. Hence, it is proved that under the proposed virtual control law $x_{(2j+1)d}$, z_{2j} is converging and bounded to

$$\Omega_{z(2j)} = \left\{ z_{2j} \in R \left| |z_{2j}| \le \sqrt{\frac{\frac{\sigma_{(2j)0}}{2}z_{2j+1}^2 + \Gamma_{2j}}{k_{2j} - \frac{1}{2\sigma_{(2j)0}} - \frac{1}{2\sigma_{(2j)5}} - \frac{\chi_{2j}^2}{2\varsigma_{2j}^2}}} \right. \right\}.$$

Step n−1: The time derivative of z_{n-1} is derived as

$$\dot{z}_{n-1} = \dot{x}_{n-1} - \dot{x}_{(n-1)d} = x_n - \dot{x}_{(n-1)d} \tag{47}$$

The virtual control law x_{nd} is designed as

$$x_{nd} = -\frac{\hat{p}_{n-1}z_{n-1}}{2\varsigma_{n-1}^2} - k_{n-1}z_{n-1} \tag{48}$$

where $k_{n-1} > 0$, $\varsigma_{n-1} > 0$, $\hat{p}_{n-1}$ is the adaptive term with following updating law

$$\dot{\hat{p}}_{n-1} = \frac{\beta_{n-1}z_{n-1}^2}{2\varsigma_{n-1}^2} - \alpha_{n-1}\hat{p}_{n-1}, \quad \alpha_{n-1} > 0,\ \beta_{n-1} > 0 \tag{49}$$

Selecting the similar Lyapunov function candidate and deriving method with (36) and (37), one can obtain

$$\dot{V}_{n-1} \le -(k_{n-1} - \frac{1}{2\sigma_{(n-1)0}} - \frac{1}{2\sigma_{(n-1)1}} - \frac{\chi_{n-1}^2}{2\varsigma_{n-1}^2})z_{n-1}^2 + \frac{1}{2\sigma_{(n-1)0}}z_n^2 + \Gamma_{n-1} \tag{50}$$

where, $\Gamma_{n-1} = \frac{\sigma_{(n-1)1}}{2}\chi_{n-1}^2 + \frac{\alpha_{n-1}}{4\beta_{n-1}}\chi_{n-1}^4$, and the parameters are chosen to guarantee $k_{n-1} - \frac{1}{2\sigma_{(n-1)0}} - \frac{1}{2\sigma_{(n-1)1}} - \frac{\chi_{n-1}^2}{2\varsigma_{n-1}^2} > 0$.

Therefore, similar conclusion can be drawn: under the proposed virtual control input x_{nd}, the state tracking error z_{n-1} is converging and bounded to a specified compact set $\Omega_{z(n-1)}$ which can be defined by $\Omega_{z(n-1)} = \left\{ z_{n-1} \in R \left| |z_{n-1}| \le \sqrt{\frac{\frac{1}{2\sigma_{(n-1)0}}z_n^2 + \Gamma_{n-1}}{k_{n-1} - \frac{1}{2\sigma_{(n-1)0}} - \frac{1}{2\sigma_{(n-1)1}} - \frac{\chi_{n-1}^2}{2\varsigma_{n-1}^2}}} \right. \right\}$.

Step n: Unconstrained control law design without considering input saturation.

Without considering input uncertainty caused by saturation and utilizing optimal RRBFNN, the time derivative of state variable x_n is rewritten as

$$\dot{x}_n = gu + f_n + \mathbf{W}_n^{*T}\mathbf{\Phi}_n + \varepsilon_n^* + d_n \tag{51}$$

where $\mathbf{W}_n^{*T}\mathbf{\Phi}_n$ is the optimal RRBFNN to approximate modeling error Δf_n, ε_n^* is the smallest approximation error of modeling error Δf_n.

The tracking error dynamics of subsystem n is derived as

$$\dot{z}_n = gu + f_n + \mathbf{W}_n^{*T}\mathbf{\Phi}_n + \varepsilon_n^* + d_n - \dot{x}_{nd} \tag{52}$$

To improve the system robustness and rate of convergence, terminal sliding mode control method is employed. An integral sliding mode surface is established with following structure:

$$s = z_n + \lambda\int_0^t z_n dt \tag{53}$$

where $\lambda > 0$ is the designed parameter.

Based on (52) and (53), the time derivative of sliding mode surface is obtained as:

$$\dot{s} = gu + f_n + \mathbf{W}_n^{*T}\mathbf{\Phi}_n + \varepsilon_n^* + d_n - \dot{x}_{nd} + \lambda z_n \tag{54}$$

To compensate for the model uncertainties, following integrated estimation function is utilized.

$$IE_n = \hat{\mathbf{W}}_n^T\mathbf{\Phi}_n + \hat{\varepsilon}_n + \hat{d}_n + \frac{\hat{\delta}_n^2 z_n}{\left|\hat{\delta}_n z_n\right| + c_n e^{-a_n t}} \tag{55}$$

where $\hat{\mathbf{W}}_n^T\mathbf{\Phi}_n$ is utilized to approximate Δf_n, and $\hat{\mathbf{W}}_n^T$ is the designed weight matrix, $\hat{\varepsilon}_n$ is the estimation of ε_n^*, $\hat{d}_n$ is the disturbance observer utilized to estimate d_n, $\frac{\hat{\delta}_n^2 z_n}{\left|\hat{\delta}_n z_n\right| + c_n e^{-a_n t}}$ is an adaptive robust term designed to compensate for the observation error $\tilde{d}_n$, and $\hat{\delta}_n$ is the estimation of $\tilde{d}_n$, $a_n > 0$, $c_n > 0$.

The disturbance observer is designed as follows.

$$\begin{aligned} \hat{d}_n &= \varphi_n + \lambda_n x_n \\ \dot{\varphi}_n &= -\lambda_n(gu + f_n + \hat{\mathbf{W}}_n^T\mathbf{\Phi}_n + \hat{d}_n) \end{aligned} \tag{56}$$

where $\hat{d}_n$ is the disturbance estimation, φ_n is the auxiliary variable, and $\lambda_n > 0$ is the designed parameter.

To improve the convergence efficiency and make the system states evolve on the given sliding manifold, following terminal reaching law is employed:

$$\dot{s} = -\tau s - \sigma\,|s|^r\,sign(s) \tag{57}$$

where $\tau > 0, \sigma > 0, 0 < r < 1$.

The actual control law u is designed as

$$u = \frac{1}{g}[-\tau s - \sigma\,|s|^r\,sign(s) - f_n - IE_n - \frac{\hat{p}_n s}{2\varsigma_n^2} - \lambda z_n] \tag{58}$$

where $\hat{p}_n$ is the adaptive term designed for $\dot{x}_{nd}$.

Moreover, the parameter updating laws are designed as

$$\begin{aligned}\dot{\hat{\mathbf{W}}}_n &= r_{n1} s \boldsymbol{\Phi}_n \\ \dot{\hat{\varepsilon}}_n &= r_{n2} s \\ \dot{\hat{\delta}}_n &= r_{n4} s \\ \dot{\hat{p}}_n &= \frac{\beta_n s^2}{2\varsigma_n^2} - \alpha_n \hat{p}_n \end{aligned} \tag{59}$$

where $r_{n1} > 0$, $r_{n2} > 0$, $r_{n4} > 0$, $\alpha_n > 0$, $\beta_n > 0$.

Theorem 3: Utilizing integrated estimation function (55), actual control law (58), and parameter updating law (59), the subsystem discussed is step n is converged, and the state tracking error z_n is guaranteed to converge to a specified compact set.

Proof 3: Consider the following Lyapunov function candidate

$$\begin{aligned} V_n = \frac{1}{2}s^2 + \frac{1}{2r_{n1}}\tilde{\mathbf{W}}_n^T\tilde{\mathbf{W}}_n + \frac{1}{2r_{n2}}\tilde{\varepsilon}_n^2 + \frac{1}{2r_{n3}}\tilde{d}_n^2 \\ + \frac{1}{2r_{n4}}\tilde{\delta}_n^2 + \frac{1}{2\beta_n}(\chi_n^2 - \hat{p}_n)^2 + \frac{c_n}{a_n}e^{-a_n t} \end{aligned} \tag{60}$$

where $\tilde{\varepsilon}_u = \varepsilon_u^* - \hat{\varepsilon}_u$, $\tilde{\varepsilon}_n = \varepsilon_n^* - \hat{\varepsilon}_n$, $\tilde{\delta}_n = \tilde{d}_n - \hat{\delta}_n$, $r_{n5} > 0$.

The time derivative of V_n is derived as

$$\begin{aligned} \dot{V}_n = s[gu + f_n + \mathbf{W}_n^{*T}\boldsymbol{\Phi}_n + \varepsilon_n^* + d_n - \dot{x}_{nd} + \lambda z_n] \\ + \frac{1}{r_{n1}}\tilde{\mathbf{W}}_n^T(\dot{\mathbf{W}}_n^* - \dot{\hat{\mathbf{W}}}_n) + \frac{1}{r_{n2}}\tilde{\varepsilon}_n(\dot{\varepsilon}_n^* - \dot{\hat{\varepsilon}}_n) + \frac{1}{r_{n3}}\tilde{d}_n(\dot{d}_n - \dot{\hat{d}}_n) \\ + \frac{1}{r_{n4}}\tilde{\delta}_n(\dot{\bar{d}}_n - \dot{\hat{\delta}}_n) - \frac{\dot{\hat{p}}_n}{\beta_n}(\chi_n^2 - \hat{p}_n) - c_n e^{-a_n t} \end{aligned} \tag{61}$$

Substituting (58-59) into (61), one can obtain

$$\begin{aligned} \dot{V}_n &= -\tau s^2 - \sigma\,|s|^{r+1} + s\tilde{d}_n + \frac{1}{r_{n3}}\tilde{d}_n\dot{d}_n - \frac{\lambda_n}{r_{n3}}\tilde{d}_n\tilde{\mathbf{W}}_n^T\boldsymbol{\Phi}_n \\ &\quad - \frac{\lambda_n}{r_{n3}}\tilde{d}_n\varepsilon_n^* - \frac{\lambda_n}{r_{n3}}\tilde{d}_n^2 + \frac{1}{r_{n4}}\tilde{\delta}_n\dot{\bar{d}}_n - \tilde{\delta}_n s - s\dot{x}_{nd} - \frac{\chi_n^2 s^2}{2\varsigma_n^2} \\ &\quad + \frac{\alpha_n\hat{p}_n}{\beta_n}\chi_n^2 - \frac{\alpha_n}{\beta_n}\hat{p}_n^2 - \frac{\hat{\delta}_n^2 s^2}{\left|\hat{\delta}_n s\right| + c_n e^{-a_n t}} - c_n e^{-a_n t} \\ &\le -\tau s^2 - \sigma\,|s|^{r+1} + \frac{1}{r_{n3}}\tilde{d}_n\dot{d}_n - \frac{\lambda_n}{r_{n3}}\tilde{d}_n\tilde{\mathbf{W}}_n^T\Phi_n - \frac{\lambda_n}{r_{n3}}\tilde{d}_n\varepsilon_n^* \\ &\quad - \frac{\lambda_n}{r_{n3}}\tilde{d}_n^2 + \frac{1}{r_{n4}}\tilde{\delta}_n\dot{\bar{d}}_n - s\dot{x}_{nd} - \frac{\chi_n^2 s^2}{2\varsigma_n^2} + \frac{\alpha_n\hat{p}_n}{\beta_n}\chi_n^2 \\ &\quad - \frac{\alpha_n}{\beta_n}\hat{p}_n^2 - \frac{c_n^2 e^{-2a_n t}}{\left|\hat{\delta}_n s\right| + c_n e^{-a_n t}} \\ &\le -\tau s^2 - \sigma\,|s|^{r+1} + \frac{1}{r_{n3}}\tilde{d}_n\dot{d}_n - \frac{\lambda_n}{r_{n3}}\tilde{d}_n\tilde{\mathbf{W}}_n^T\boldsymbol{\Phi}_n - \frac{\lambda_n}{r_{n3}}\tilde{d}_n\varepsilon_n^* \\ &\quad - \frac{\lambda_n}{r_{n3}}\tilde{d}_n^2 + \frac{1}{r_{n4}}\tilde{\delta}_n\dot{\bar{d}}_n - s\dot{x}_{nd} - \frac{\chi_n^2 s^2}{2\varsigma_n^2} + \frac{\alpha_n\hat{p}_n}{\beta_n}\chi_n^2 - \frac{\alpha_n}{\beta_n}\hat{p}_n^2 \end{aligned} \tag{62}$$

Considering the constraints $|\phi_n| \le 1$, $\left|\varepsilon_n^*\right| \le \bar{\varepsilon}_n$, and $\left|\dot{d}_n\right| \le \bar{d}_{cn}$, the time derivative of V_n can be further derived as

$$\begin{aligned} \dot{V}_n &\le -\tau s^2 - \sigma\,|s|^{r+1} + \frac{1}{r_{n3}}\left|\tilde{d}_n\right|\left|\bar{d}_{cn}\right| + \frac{\lambda_n}{r_{n3}}\left|\tilde{d}_n\right|\left|\tilde{\mathbf{W}}_n^T\right| \\ &\quad + \frac{\lambda_n}{r_{n3}}\left|\tilde{d}_n\right|\left|\bar{\varepsilon}_n\right| - \frac{\lambda_n}{r_{n3}}\tilde{d}_n^2 + \frac{1}{r_{n4}}\left|\tilde{\delta}_n\right|\left|\dot{\bar{d}}_n\right| + |s|\,|\dot{x}_{nd}| \\ &\quad - \frac{\chi_n^2 s^2}{2\varsigma_n^2} + \frac{\alpha_n\hat{p}_n}{\beta_n}\chi_n^2 - \frac{\alpha_n}{\beta_n}\hat{p}_n^2 \\ &\le -\tau s^2 - \sigma\,|s|^{r+1} + \frac{1}{2\sigma_{n1}}\frac{1}{r_{n3}}\tilde{d}_n^2 + \frac{\sigma_{n1}}{2}\frac{1}{r_{n3}}\bar{d}_{cn}^2 + \frac{1}{2\sigma_{n2}}\frac{\lambda_n}{r_{n3}}\tilde{d}_n^2 \\ &\quad + \frac{\sigma_{n2}}{2}\frac{\lambda_n}{r_{n3}}\tilde{\mathbf{W}}_n^T\tilde{\mathbf{W}}_n + \frac{1}{2\sigma_{n3}}\frac{\lambda_n}{r_{n3}}\tilde{d}_n^2 + \frac{\sigma_{n3}}{2}\frac{\lambda_n}{r_{n3}}\bar{\varepsilon}_n^2 - \frac{\lambda_n}{r_{n3}}\tilde{d}_n^2 \\ &\quad + \frac{1}{2\sigma_{n4}r_{n4}}\tilde{\delta}_n^2 + \frac{\sigma_{n4}}{2}\frac{1}{r_{n4}}\dot{\bar{d}}_n^2 + \frac{1}{2\sigma_{n5}}s^2 + \frac{\sigma_{n5}}{2}\chi_n^2 - \frac{\chi_n^2 s^2}{2\varsigma_n^2} \\ &\quad + \frac{\alpha_n\hat{p}_n}{\beta_n}\chi_n^2 - \frac{\alpha_n}{\beta_n}\hat{p}_n^2 \\ &= -(\tau - \frac{1}{2\sigma_{n5}} + \frac{\chi_n^2}{2\varsigma_n^2})s^2 - \sigma\,|s|^{r+1} + \Gamma_n \end{aligned} \tag{63}$$

where $\sigma_{ni}, i = 1, 2, 3, 4, 5$ are positive constants, and the parameters are chosen to satisfy $\tau - \frac{1}{2\sigma_{n5}} + \frac{\chi_n^2}{2\varsigma_n^2} > 0$ and $\frac{\lambda_n}{r_{n3}} - \frac{1}{2\sigma_{n1}r_{n3}} - \frac{\lambda_n}{2\sigma_{n2}r_{n3}} - \frac{\lambda_n}{2\sigma_{n3}r_{n3}} \ge 0$. Γ_n is a defined auxiliary variable, and it is expressed as follows.

$$\begin{aligned} \Gamma_n = \frac{\sigma_{n2}}{2}\frac{\lambda_n}{r_{n3}}\tilde{\mathbf{W}}_n^T\tilde{\mathbf{W}}_n + \frac{1}{2\sigma_{n4}r_{n4}}\tilde{\delta}_n^2 + \frac{\sigma_{n4}}{2}\frac{1}{r_{n4}}\dot{\bar{d}}_n^2 \\ + \frac{\sigma_{n1}}{2}\frac{1}{r_{n3}}\bar{d}_{cn}^2 + \frac{\sigma_{n3}}{2}\frac{\lambda_n}{r_{n3}}\bar{\varepsilon}_n^2 + \frac{\sigma_{n5}}{2}\chi_n^2 + \frac{\alpha_n}{4\beta_n}\chi_n^4. \end{aligned}$$

Obviously, it can be concluded from (63) that $\dot{V}_n < 0$ as long as $s^2 > \Gamma_n \Big/ (\tau - \frac{1}{2\sigma_{n5}} + \frac{\chi_n^2}{2\varsigma_n^2})$ or $|s|^{r+1} > \Gamma_n/\sigma$. Consequently, the decrease of V_n will drive s into the boundary $|s| \le \sqrt{\Gamma_n \Big/ (\tau - \frac{1}{2\sigma_{n5}} + \frac{\chi_n^2}{2\varsigma_n^2})}$ or $|s| \le \sqrt[r+1]{\Gamma_n/\sigma}$.

Therefore, it is proved that under the proposed control law u, the sliding mode surface s is bounded to a specified compact set as

$$\Omega_s = \{s \in R \,||s| \le \zeta\} \tag{64}$$

where $\zeta = \min\left(\sqrt{\Gamma_n \Big/ (\tau - \frac{1}{2\sigma_{n5}} + \frac{\chi_n^2}{2\varsigma_n^2})},\ \sqrt[r+1]{\Gamma_n/\sigma}\right)$.

Based on (53), following equation can be obtained.

$$z_n(t) = s(t) - \lambda e^{-\lambda t}\int_0^t s(\varpi)e^{\lambda\varpi}\,d\varpi \tag{65}$$

Considering the boundary of s presented in (64), one can obtain

$$\begin{aligned} |z_n| &\le |s| + \lambda e^{-\lambda t}\int_0^t |s(\varpi)|\,e^{\lambda\varpi}\,d\varpi \\ &\le \zeta + \lambda e^{-\lambda t}\int_0^t \zeta e^{\lambda\varpi}\,d\varpi \\ &= \zeta(1 + \lambda e^{-\lambda t}\int_0^t e^{\lambda\varpi}\,d\varpi) \\ &= \zeta(2 - e^{-\lambda t}) \\ &\le 2\zeta \end{aligned} \tag{66}$$

Therefore, it is proved that under the proposed control law u, the state variable z_n is bounded to a specified compact set as

$$\Omega_{z_n} = \{z_n \in R \,||z_n| \le 2\zeta\} \tag{67}$$

Step n+1: Constrained control law design considering input saturation.

To solve the problem of input saturation, we employ the anti-windup compensator [41]–[43] as

$$\dot{w} = \begin{cases} -kw - \dfrac{|gs\Delta u| + \frac{1}{2}(\Delta u)^2}{|w|^2} w + \Delta u & |w| \ge \mu \\ 0 & |w| < \mu \end{cases} \tag{68}$$

where w is the state of the auxiliary design system, $k > 0$ is a designed parameter, μ is a small positive designed parameter.

Considering the input saturation, the actual control law u is redesigned as

$$u = \frac{1}{g}[-\tau s + w - \sigma\,|s|^r\, sign(s) - f_n - IE_n - \frac{\hat{p}_n s}{2\varsigma_n^2} - \lambda z_n] \tag{69}$$

where IE_n is same with (55), and the parameter updating laws are same with (59).

The disturbance observer utilized in IE_n is redesigned as

$$\begin{aligned} \hat{d}_n &= \varphi_n + \lambda_n x_n \\ \dot{\varphi}_n &= -\lambda_n(gu + g\Delta u + f_n + \hat{\mathbf{W}}_n^T \mathbf{\Phi}_n + \hat{d}_n) \end{aligned} \tag{70}$$

Theorem 4: Utilizing anti-windup compensator (68) and actual control law (69), the effect of input saturation is restricted, and the state tracking error z_n is guaranteed to converge to a specified compact set.

Proof 4: Considering input saturation, the tracking dynamics of subsystem n are expressed as

$$\begin{aligned} \dot{x}_n &= gu + g\Delta u + f_n + \mathbf{W}_n^{*T}\mathbf{\Phi}_n + \varepsilon_n^* + d_n \\ \dot{z}_n &= gu + g\Delta u + f_n + \mathbf{W}_n^{*T}\mathbf{\Phi}_n + \varepsilon_n^* + d_n - \dot{x}_{nd} \end{aligned} \tag{71}$$

Consider the following Lyapunov function candidate

$$V_{n+1} = V_n + \frac{1}{2}w^2 \tag{72}$$

The time derivative of V_{n+1} is derived as

$$\begin{aligned} \dot{V}_{n+1} = {} & s[gu + g\Delta u + f_n + \mathbf{W}_n^{*T}\mathbf{\Phi}_n + \varepsilon_n^* + d_n - \dot{x}_{nd} + \lambda z_n] \\ & + \frac{1}{r_{n1}}\tilde{\mathbf{W}}_n^T(\dot{\mathbf{W}}_n^* - \dot{\hat{\mathbf{W}}}_n) + \frac{1}{r_{n2}}\tilde{\varepsilon}_n(\dot{\varepsilon}_n^* - \dot{\hat{\varepsilon}}_n) \\ & + \frac{1}{r_{n3}}\tilde{d}_n(\dot{d}_n - \dot{\hat{d}}_n) + \frac{1}{r_{n4}}\tilde{\delta}_n(\dot{\tilde{d}}_n - \dot{\hat{\delta}}_n) \\ & - \frac{\dot{\hat{p}}_n}{\beta_n}(\chi_n^2 - \hat{p}_n) - c_n e^{-a_n t} + w\dot{w} \end{aligned} \tag{73}$$

Combining with previous deriving result in Theorem 3, one can obtain

$$\begin{aligned} \dot{V}_{n+1} \le {} & -(\tau - \frac{1}{2\sigma_{n5}} + \frac{\chi_n^2}{2\varsigma_n^2})s^2 - \sigma\,|s|^{r+1} \\ & + \Gamma_n + ws + gs\Delta u + w\dot{w} \\ = {} & -(\tau - \frac{1}{2\sigma_{n5}} + \frac{\chi_n^2}{2\varsigma_n^2})s^2 - \sigma\,|s|^{r+1} \\ & + \Gamma_n + ws + gs\Delta u - kw^2 \\ & - |gs\Delta u| - \frac{1}{2}(\Delta u)^2 + w\Delta u \\ \le {} & -(\tau - \frac{1}{2\sigma_{n5}} + \frac{\chi_n^2}{2\varsigma_n^2})s^2 - \sigma\,|s|^{r+1} + \Gamma_n \\ & + \frac{1}{2\sigma_{n6}}w^2 + \frac{\sigma_{n6}}{2}s^2 \\ & - (k - \frac{1}{2})w^2 - \frac{1}{2}(w - \Delta u)^2 \\ \le {} & -(\tau - \frac{1}{2\sigma_{n5}} - \frac{\sigma_{n6}}{2} + \frac{\chi_n^2}{2\varsigma_n^2})s^2 - \sigma\,|s|^{r+1} + \Gamma_n \end{aligned} \tag{74}$$

where σ_{n6} are designed positive constants, and the parameters are chosen to satisfy the condition $\tau - \frac{1}{2\sigma_{n5}} - \frac{\sigma_{n6}}{2} + \frac{\chi_n^2}{2\varsigma_n^2} > 0$ and $k - \frac{1}{2} - \frac{1}{2\sigma_{n6}} \ge 0$.

Utilizing the same deriving method in Theorem 3, the convergence of subsystem n can be guaranteed, and the boundaries of s and z_n can be expressed as

$$\begin{aligned} \Omega_s &= \{s \in R \,||s| \le \zeta\} \\ \Omega_{z_n} &= \{z_n \in R \,||z_n| \le 2\zeta\} \end{aligned} \tag{75}$$

where $\zeta = \min\left(\sqrt{\Gamma_n \Big/ (\tau - \frac{1}{2\sigma_{n5}} - \frac{\sigma_{n6}}{2} + \frac{\chi_n^2}{2\varsigma_n^2})},\ \sqrt[r+1]{\Gamma_n/\sigma}\right)$.

Theorem 5: Under the proposed control scheme, the uniformly ultimately bounded convergences of all closed-loop signals are guaranteed.

Proof 5: It has been proved that utilizing the designed virtual control laws and actual control law, the state tracking errors $z_i, i = 1, 2, \ldots, n$ are guaranteed to converge to specified compact sets, regardless of the input uncertainties, modeling errors, and external disturbances. The boundaries of tracking errors $z_i, i = 1, 2, \ldots, n$ derived before are summarized as follows:

$$\begin{aligned} |z_1| &\le \sqrt{\frac{\sigma 10}{2}z_2^2 \Big/ (k_1 - \frac{1}{2\sigma 10})} \\ |z_2| &\le \sqrt{(\frac{\sigma_{20}}{2}z_3^2 + \Gamma_2) \Big/ (k_2 - \frac{1}{2\sigma_{20}})} \\ &\vdots \\ |z_{2j-1}| &\le \sqrt{\frac{\frac{1}{2\sigma_{(2j-1)0}}z_{2j}^2 + \Gamma_{2j-1}}{k_{2j-1} - \frac{1}{2\sigma_{(2j-1)0}} - \frac{1}{2\sigma_{(2j-1)1}} - \frac{\chi_{2j-1}^2}{2\varsigma_{2j-1}^2}}} \\ |z_{2j}| &\le \sqrt{\frac{\frac{\sigma_{(2j)0}}{2}z_{2j+1}^2 + \Gamma_{2j}}{k_{2j} - \frac{1}{2\sigma_{(2j)0}} - \frac{1}{2\sigma_{(2j)5}} - \frac{\chi_{2j}^2}{2\varsigma_{2j}^2}}} \\ &\vdots \end{aligned}$$

$$|z_{n-1}| \leq \sqrt{\frac{\frac{1}{2\sigma_{(n-1)0}} z_n^2 + \Gamma_{n-1}}{k_{n-1} - \frac{1}{2\sigma_{(n-1)0}} - \frac{1}{2\sigma_{(n-1)1}} - \frac{\chi_{n-1}^2}{2\varsigma_{n-1}^2}}}$$

$$|z_n| \leq 2 \min\left(\sqrt{\Gamma_n \Big/ (\tau - \frac{1}{2\sigma_{n5}} - \frac{\sigma_{n6}}{2} + \frac{\chi_n^2}{2\varsigma_n^2})}, \sqrt[r+1]{\Gamma_n / \sigma} \right)$$

As shown in (76), the boundaries of $|z_i|, i = 1, \ldots, n-1$ are related to the values of their next tracking errors z_{i+1}, $i = 1, \ldots, n-1$. According to previous analysis, $\Gamma_i, i = 2, \ldots, n$ is bounded, therefore, z_n is guaranteed to be converged, and then z_{n-1} is converged. Consequently, $z_i, i = 1, \ldots, n-2$ are converged. Hence, the uniformly ultimately bounded convergences of all closed-loop signals are guaranteed. Moreover, the tracking errors can be guaranteed to converge to small neighborhoods of the origin by choosing the designed parameters appropriately.

Chattering Problem Handling: Chattering is a well-known problem with sliding mode control, which is usually caused by the utilization of the discontinuous function $sign(s)$. In this paper, the chattering problem is not serious since the gain parameter of $sign(s)$ is $\sigma |s|^r$ (see equation (69)), which is related to the value of s. When the sliding surface is switching near zero, the gain parameter $\sigma |s|^r$ is very small, so the influence of chattering problem is greatly reduced.

However, this doesn't solve the chattering problem completely. To annihilate the chattering problem, the discontinuous function $sign(s)$ in the control input (69) is replaced by following saturation function:

$$sat(s) = \begin{cases} \frac{s}{|s|} & if\ s > \Psi \\ \frac{s}{\Psi} & if\ s \leq \Psi \end{cases} \tag{76}$$

where Ψ is the boundary layer introduced around the sliding surface $s = 0$.

Utilizing the saturation function $sat(s)$, the high frequency switching phenomenon around $s = 0$ is avoided. Hence, the chattering problem can be solved.

IV. SIMULATION

A. SIMULATION PREPARATION

Numerical simulations of trajectory tracking of a 6th order cable-driven vehicle model system are carried out in this section. The parameters of simulation model are presented in Table 1. The performance of the proposed controller is compared with two other control methods viz. (a) adaptive backstepping terminal sliding mode control, (b) integrated estimation based backstepping control, as shown in Table 2. A-BTSMC utilizes adaptive terms to replace RRBFNN and DO for uncertainties compensations, which can be given by $\frac{\hat{\varphi}_i^2 z_i}{\hat{\varphi}_i |z_i| + \tau_i e^{-n_i t}}$, and the adaptive law is chosen as $\dot{\hat{\varphi}}_i = r_i |z_i|$. I-BC utilizes conventional backstepping control law rather than terminal sliding mode control law at the final step of controller design.

TABLE 1. The parameters of simulation model.

Parameter	Definition	Value	Unit
M	Mass of the vehicle	100	kg
ΔM	Added mass	10	kg
C_d	Drag force coefficient	0.1	/
ρ	Water density	998.2	kg/m^3
A	Sectional area of vehicle	0.5	m^2
$K_{il}, i=1,2,3$	Cable stiffness coefficients	250	N/m
$K_{i2}, i=1,2,3$	Cable stiffness coefficients	120	N/m^3
R	Radius of winch and wheel	1	m
J_1	Moment of inertia of winch	200	kg·m^2
J_2	Moment of inertia of wheel	100	kg·m^2
μ	Frictional coefficient	0.15	/
g	Acceleration of gravity	10	m/s^2
n	Reduction ratio	200	/

TABLE 2. Control methods utilized in the simulation.

Method	Description
I-BTSMC	Proposed control
A-BTSMC	Adaptive backstepping terminal sliding mode control
I-BC	Integrated estimation based backstepping control

The backstepping terminal sliding mode control parameters of I-BTSMC are selected as $k_1 = 12, k_2 = 2.5, k_3 = 2.0, k_4 = 0.5, k_5 = 0.9, \lambda = 15, \tau = 5, \sigma = 5, r = 0.8, \Psi = 0.1$. The adopted RRBFNN contains five nodes in the hidden layer, gains of weight matrix are set to $r_{21} = 0.1$, $r_{41} = 1.2$, $r_{61} = 0.5$, and the connection weight between output layer and hidden layer is selected as $v = 1$. The parameters of disturbance observers are selected as $\lambda_2 = \lambda_4 = \lambda_6 = 15$. The adaptive parameters used for estimation error compensation are set to $r_{23} = r_{24} = r_{43} = r_{44} = r_{62} = r_{64} = 0.01, c_2 = c_4 = c_6 = 1, a_2 = a_4 = a_6 = 0.1$. The parameters of adaptive functions used for $\dot{x}_{id}, i = 3, 4, 5, 6$ compensation are selected as $\alpha_i = \beta_i = 0.1, i = 3, 4, 5, 6$, $\varsigma_i = 1, i = 3, 4, 5, 6$. The magnitude of the input saturation limit is set to $\tau_m = 500$. The parameters of adaptive terms used in A-BTSMC are designed as $r_i = 0.02, \tau_i = 1$, $n_i = 0.15$. Conventional backstepping control is utilized at the final step of I-BC, and the control gain is selected as $k_6 = 25$.

B. CASE 1: UNIFORM TRAJECTORY TRACKING CONTROL UNDER SIMPLE UNCERTAINTIES

In case 1, the vehicle is required to achieve uniform motion tracking control under time-varying multisource unknown uncertainties. The reference trajectory is selected as $x_{1d}(t) = 1 + t$. Time-varying uncertainties are selected as $d_2(t) = \sin(0.5t) + 1, d_4(t) = 1.5\sin(t) + 1, d_6(t) = 3\sin(2t) + 3, \Delta f_2(t) = \Delta f_4(t) = \Delta f_6(t) = 0.01\cos(t)$. Initial conditions are set to $\mathbf{x}(0) = [\,0\ 0\ 0\ 0\ 0\ 0\,]^T$.

The trajectory tracking results are presented in Fig. 6. It is seen that the vehicle can converge to and move

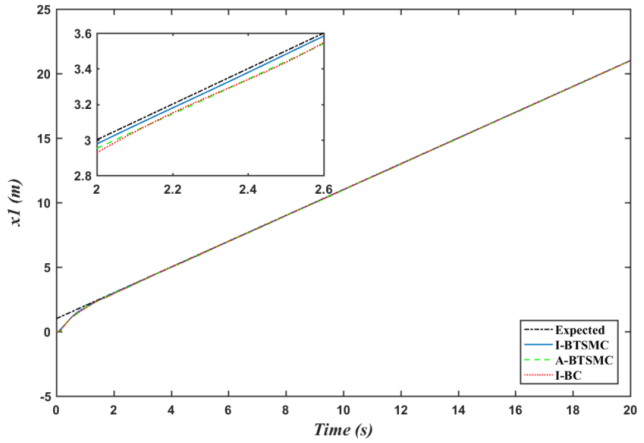

FIGURE 6. Tracking trajectories of case 1.

along the desired trajectory regardless of multisource time-varying uncertainties. Moreover, the locally enlarged image in Fig. 6 shows that the tracking performance of proposed controller is better than A-BTSMC and I-BC.

The tracking errors of all the variables are demonstrated in Figs. 7-8. It is shown that the tracking errors of I-BTSMC are smaller than A-BTSMC and I-BC. Besides, the tracking errors of I-BTSMC are more stable, whereas significant vibrations are observed in the transient phase for I-BC, and low frequency oscillations occur in the steady state for A-BTSMC.

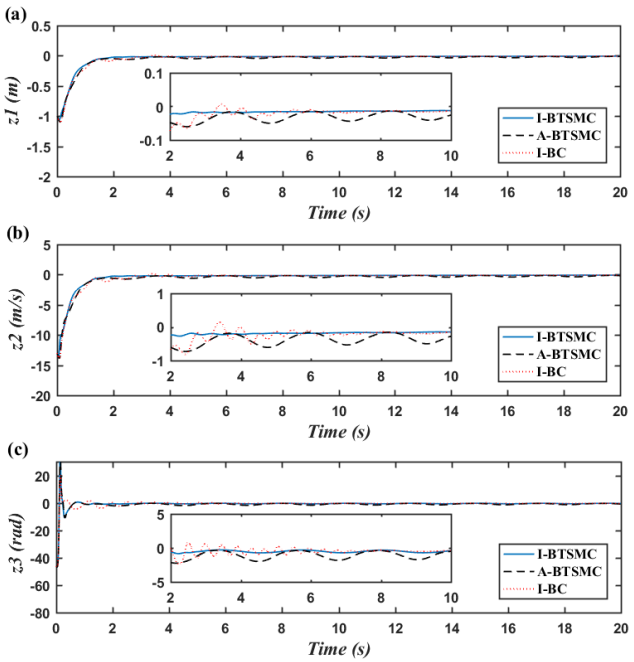

FIGURE 7. The first three tracking errors of case 1.

To further illustrate the differences of tracking performances of the three control methods, data comparisons of the three control methods in steady-state stage are shown

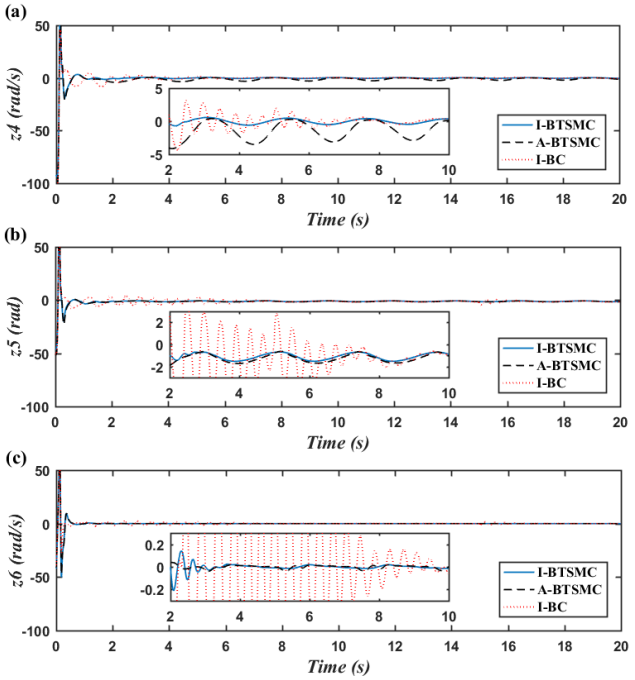

FIGURE 8. The last three tracking errors of case 1.

in Figs. 9-10. Among the three kinds of data, absolute mean value reflects the control precision, maximum absolute value and mean square error reflect the stability and fluctuation range of tracking errors. Apparently, the control precision and stability of I-BTSMC in steady-state is better than A-BTSMC and I-BC.

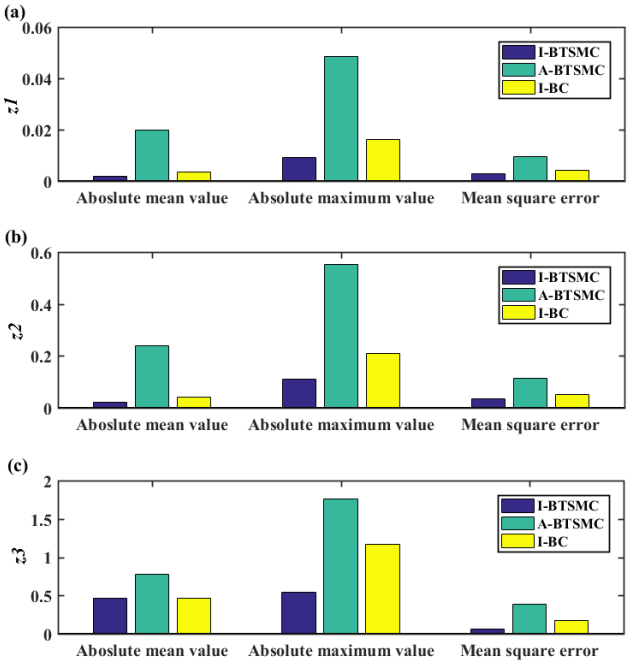

FIGURE 9. Data analysis of the first three tracking errors of case 1.

Moreover, the performances of external disturbances estimations are shown in Fig. 11. It is shown that the proposed

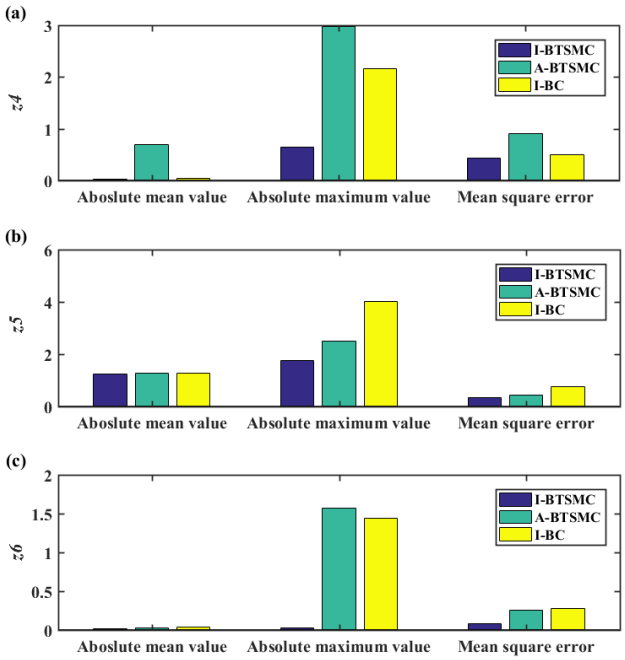

FIGURE 10. Data analysis of the last three tracking errors of case 1.

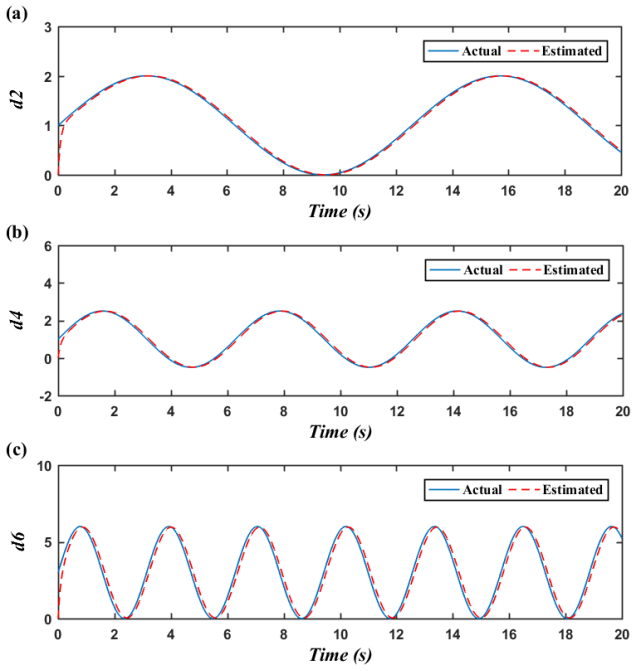

FIGURE 11. External disturbance estimation of case 1.

method can achieve perfect estimations of the external disturbances. The control input of case 1 is shown in Fig. 12. It is seen that the control input without a compensator hit the bound of the actuator and suffer from chattering at the beginning of the simulation, whereas the performance has been improved by anti-windup compensator.

Hence, from the aforementioned simulation results in case 1, we may draw the conclusion that the performance

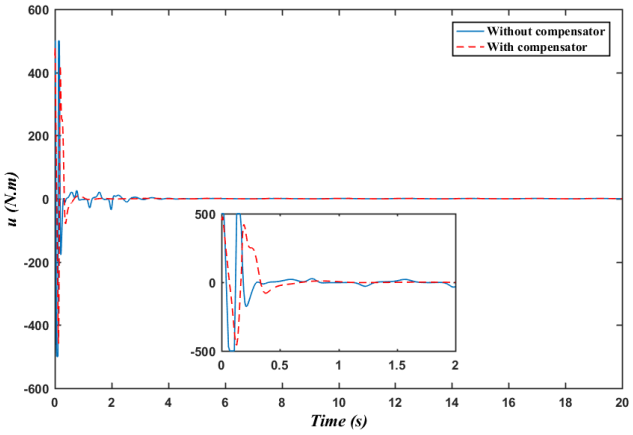

FIGURE 12. Control input of case 1.

of I-BTSMC is better than A-BTSMC and I-BC for uniform motion tracking control under multisource time-varying uncertainties.

C. CASE 2: INTEGRATED TRAJECTORY TRACKING CONTROL UNDER COMPLEX UNCERTAINTIES

In case 2, the cable-driven vehicle is required to achieve integrated motion tracking control under multisource piecewise time-varying and state-dependent unknown uncertainties. Initial conditions of cable-driven vehicle model system are set to $\mathbf{x}(0) = [\,0\ 0\ 0\ 0\ 0\ 0\,]^T$. The reference trajectory is composed of three different stages viz. (a) uniformly accelerated motion, (b) uniform motion, (c) uniformly retarded motion, as shown below.

$$x_{1d}(t) = \begin{cases} 1 + 0.1t^2 & 0 \le t \le 5 \\ t - 1.5 & 5 < t \le 15 \\ -0.1t^2 + 4t - 24 & 15 < t \le 20 \end{cases}$$

The multisource piecewise time-varying and state-dependent uncertainties are selected as follows.

$$d_i(t) = \begin{cases} x_i \sin(t) & 0 \le t \le 5 \\ 1.5x_i^2 \sin(2t) + 0.1 & 5 < t \le 15, \\ 2x_i \sin(t) & 15 < t \le 20 \end{cases} \quad i = 2, 4, 6$$

$$\Delta f_i(t) = \begin{cases} 0.01x_i \cos(t) & 0 \le t \le 5 \\ 0.01x_i^2 \cos(2t) + 0.1 & 5 < t \le 15, \\ 0.01x_i \cos(t) & 15 < t \le 20 \end{cases} \quad i = 2, 4, 6$$

The trajectory tracking performances are presented in Fig. 13. The tracking errors of all the variables are demonstrated in Figs. 14-15. To further illustrate the performance difference of the three control methods, data comparisons of the three control methods in steady-state are shown in Figs. 16-17. The performances of external disturbances estimations are shown in Fig. 18.

Compared with case 1, the reference trajectory and multisource uncertainties of case 2 are more complex.

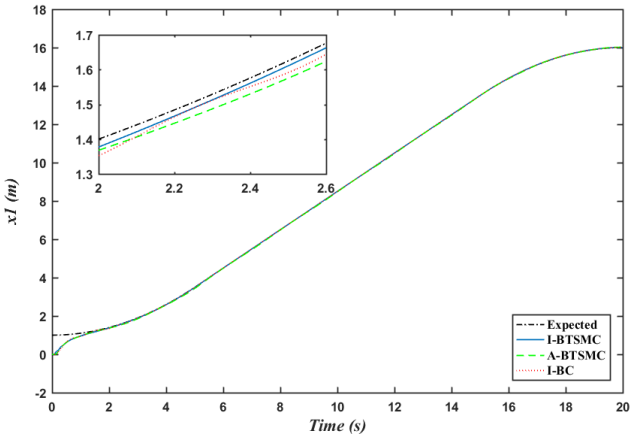

FIGURE 13. Tracking trajectories of case 2.

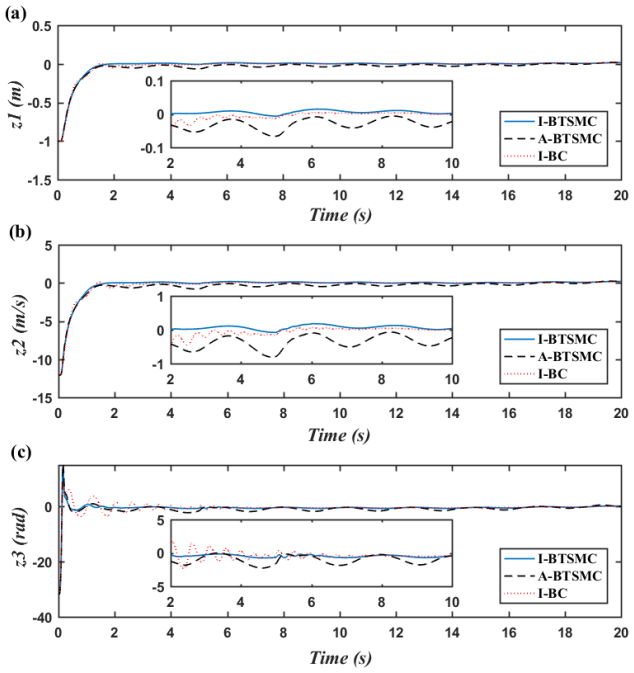

FIGURE 14. The first three tracking errors of case 2.

The unknown uncertainties of case 1 are time-varying with known upper bounds, whereas the multisource uncertainties of case 2 are not only piecewise time-varying, but also state-dependent with unknown upper bounds. Therefore, better estimating and anti-jamming capabilities are required for case 2.

From Figs. 13-17, similar conclusions can be drawn: the performance of I-BTSMC is better than A-BTSMC and I-BC with better control precision and stability. Moreover, compared with case 1, more serious oscillations are observed for A-BTSMC and I-BC, as shown in the locally enlarged images of Figs. 14-15, whereas the trend of I-BTSMC is basically consistent. Besides, it is shown by Fig. 18 that although the external disturbances have become more complex, the proposed method can still achieve good disturbance estimation.

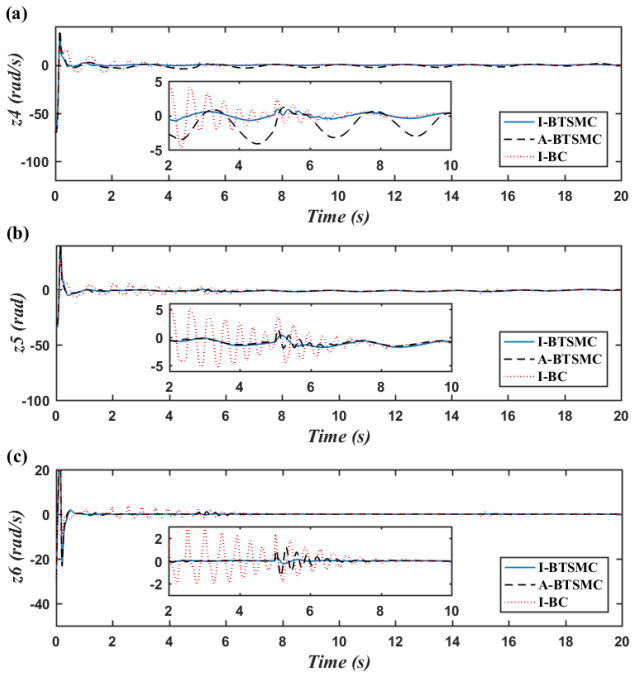

FIGURE 15. The last three tracking errors of case 2.

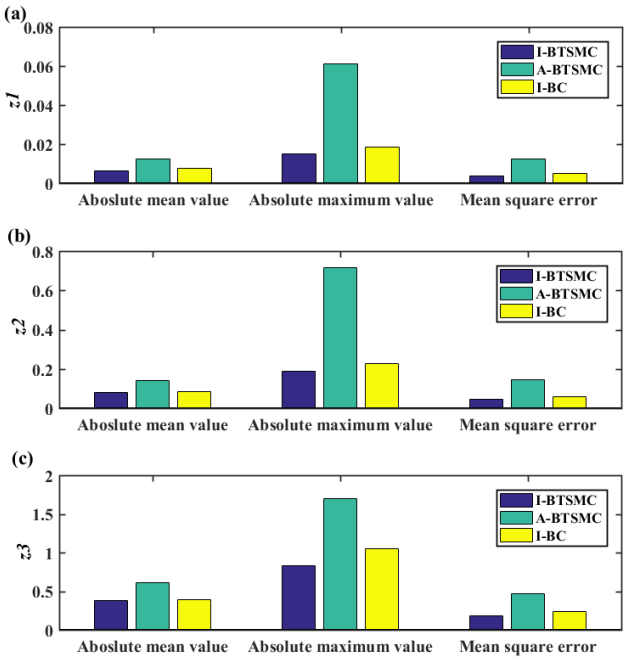

FIGURE 16. Data analysis of the first three tracking errors of case 2.

The control input of case 2 is shown in Fig. 19, which also demonstrates the effectiveness of anti-windup compensator.

From the aforementioned analyses, it can be concluded that compared with A-BTSMC and I-BC, the proposed controller performs better with higher steady-state precision, smaller oscillation, and better capability of resisting disturbance, hence, it is more suitable for cable-driven underwater vehicle control.

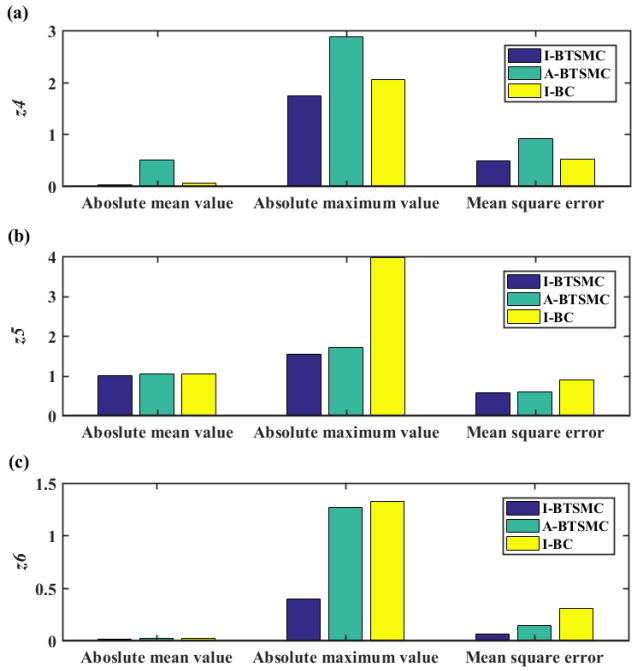

FIGURE 17. Data analysis of the last three tracking errors of case 2.

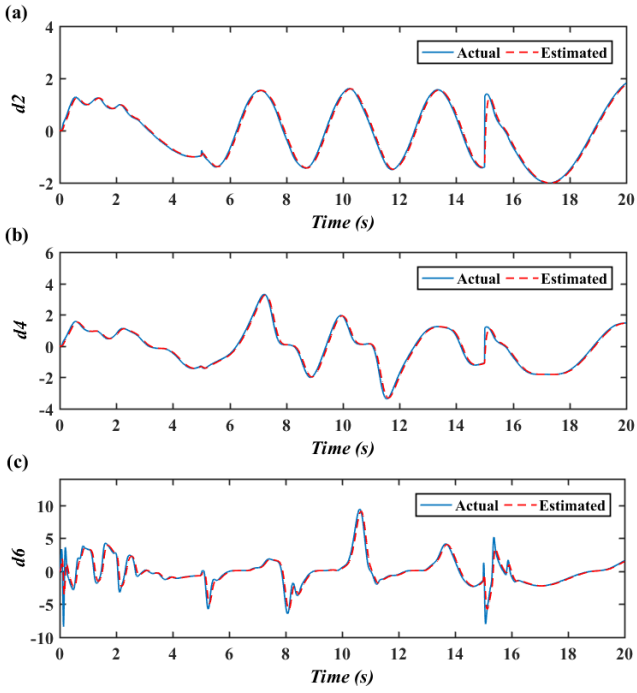

FIGURE 18. External disturbance estimation of case 2.

D. INVESTIGATION OF NONLINEAR CABLE DYNAMICS

Although accurate trajectory tracking is achieved by the proposed I-BTSMC scheme, the system variables exhibit complex nonlinear variations, especially at the beginning stage. To identify possible causes of this phenomenon, analysis of the nonlinear cable dynamics is implemented in this section.

Define the tension of cable subsection i in Fig. 2 as $F_i, i = 1, 2, 3$. The dynamic responses of $F_i, i = 1, 2, 3$ in the two simulation cases are presented in Fig. 20.

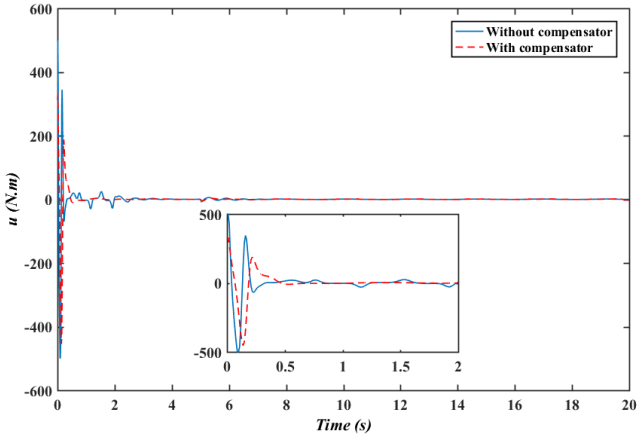

FIGURE 19. Control input of case 2.

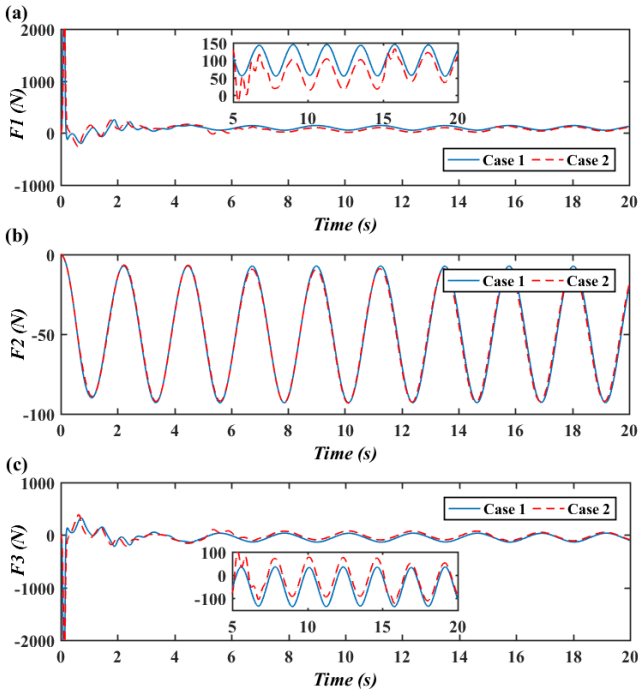

FIGURE 20. Dynamic responses of cable tensions.

From the simulation results of cable tensions, following characteristics can be summarized.

1) Nonlinear variations are observed for the overall performances of cable tensions, but the situation is particularly serious at the beginning. This phenomenon is mainly caused by the following two reasons: (1) the state of system suddenly changes from static to dynamic at the beginning, but the energy transfer in the cable takes time. As a result, the energy distribution on the cable is uneven, the energy of cable element which is in contact with the active hydraulic winch is the largest, whereas the energy of cable element which is far away from the hydraulic winch is weak; (2) the starting point of the expected trajectory is different from that of the system variable.

2) The nonlinear fluctuations of F_1 and F_3 are more complex than that of F_2 at the beginning. This phenomenon is mainly caused by the following reason: the cable subsections 1 and 3 are connected to the hydraulic winch, therefore, their dynamic behaviors change directly without any buffering once the system starts to run. Comparatively speaking, the two ends of cable subsection 2 are both connected to the passive devices; hence, the sudden change of energy is partially offset by the transfer medium.
3) Compared with case 1, the nonlinear fluctuations of case 2 are more complex, especially around 5s and 15s, when system uncertainties mutate.

Based on above analyses, it can be concluded that the sudden changes of system states and uncertainties are the main cause of nonlinear sudden change of cable dynamics, and the sudden changes are more serious for the cable subsections which are directly connected to hydraulic winch.

E. DISCUSSIONS OF THE SIMULATION RESULTS

According to the aforementioned simulation results, it is clearly shown that the proposed controller can achieve accurate and robust trajectory tracking despite the presence of nonlinear cable-drive dynamics, multisource unknown uncertainties, and input saturation. Moreover, the proposed controller exhibits better tracking accuracy and stability than two other control algorithms. Therefore, the proposed controller is proved to be effective and suitable for the cable-driven underwater vehicle control.

However, following two undesirable problems are observed: (1) The transient performance of the proposed controller still needs to be improved, especially at the initial adjusting stage; (2) The control inputs vary widely in a short time at the initial adjusting stage, which may exceed the actual response capability of the hydraulic winch.

In addition to the nonlinear cable-driven dynamics, the aforementioned two problems are mainly caused by the use of too many extra variables and the lack of parameter optimization mechanism. To deal with the multisource uncertainties and achieve the control target, too many extra variables are utilized in the control algorithm, which turns the original system into a high dimensional closed-loop system, thus the transient performance may be poor. Besides, to achieve fast convergence in initial stage and accurate trajectory tracking in steady-state, the parameters are tuned to be a little aggressive, which may bring fluctuations to the performance of initial stage.

To tackle the above two problems, the control algorithm needs to be simplified and some parameter optimization mechanism needs to be considered, which will be addressed in our future works.

V. CONCLUSIONS AND FUTURE WORK

In this paper, a new cable-driven underwater vehicle model system is proposed for future application on a tension leg platform. Firstly, a general nth order nonlinear uncertain mathematical model is established to describe the complex cable-driven dynamics. Secondly, to achieve accurate and robust trajectory tracking, an integrated estimation based adaptive backstepping terminal sliding mode controller is designed, with following critical problems considered: multisource unknown uncertainties, explosion of complexity, and input saturation. Finally, the effectiveness of the proposed control scheme is verified through plenty of numerical simulations.

Theoretically speaking, the proposed control method can apply to any unknown uncertainties as long as they are bounded, as described in Assumption 2, since the design of control algorithm does not require any knowledge of the uncertainties in advance. Utilizing the proposed control method, the known boundary requirements of uncertainties are relaxed, thus leading to better anti-jamming ability. Therefore, the control algorithm designed in this paper can be widely used for the uncertain systems in engineering applications. However, the effectiveness of the control method needs further verification when facing with more complex actual uncertainties.

Besides, although it is shown that the developed controller can achieve accurate and robust trajectory tracking despite the presence of unknown uncertainties and input saturation, following problems should be considered before the actual application:

1) In order to obtain better transient performance, the control algorithm needs to be simplified, and the parameter optimization mechanism needs to be considered.
2) More actual system constraints and uncertainties need to be considered in controller design, such as the time-varying hydraulic parameters, input delay, input dead-zone, and the actual response capability of the hydraulic winch.
3) In order to limit the fluctuations of the cable tensions and improve the stiffness of the system, mechanical tensioning device should be considered in the system.

Actually, this paper belongs to the early design stage of the cable-driven underwater vehicle system, so the aforementioned practical problems have not been considered, but the above problems will be addressed in our future works.

REFERENCES

[1] Q. Zhang, J. Zhang, A. Chemori, and X. Xiang, "Virtual submerged floating operational system for robotic manipulation," *Complexity*, vol. 2018, Nov. 2018, Art. no. 9528313. doi: 10.1155/2018/9528313.
[2] Y. Xia, K. Xu, Y. Li, G. Xu, and X. Xiang, "Improved line-of-sight trajectory tracking control of under-actuated AUV subjects to ocean currents and input saturation," *Ocean Eng.*, vol. 174, pp. 14–30, Feb. 2019.
[3] M. M. Horoub, M. Hassan, and M. A. Hawwa, "Workspace analysis of a Gough-Stewart type cable marine platform subjected to harmonic water waves," *Mechanism Mach. Theory*, vol. 120, pp. 314–325, Feb. 2018.
[4] A. R. Dehghani-Sanij, Y. S. Muzychka, and G. F. Naterer, "Droplet trajectory and thermal analysis of impinging saline spray flow on marine platforms in cold seas and ocean regions," *Ocean Eng.*, vol. 148, pp. 538–547, Jan. 2018.
[5] G. Allibert, M.-D. Hua, S. Krupínski, and T. Hamel, "Pipeline following by visual servoing for autonomous underwater vehicles," *Control Eng. Pract.*, vol. 82, pp. 151–160, Jan. 2019.

[6] X. Xiang, C. Yu, L. Lapierre, J. Zhang, and Q. Zhang, "Survey on fuzzy-logic-based guidance and control of marine surface vehicles and underwater vehicles," *Int. J. Fuzzy Syst.*, vol. 20, no. 2, pp. 572–586, Feb. 2018.

[7] Y.-F. Lu, D.-P. Fan, H. Liu, and M. Hei, "Transmission capability of precise cable drive including bending rigidity," *Mechanism Mach. Theory*, vol. 94, pp. 132–140, Dec. 2015.

[8] H. Li, W. Liu, K. Wang, K. Kawashima, and E. Magid, "A cable-pulley transmission mechanism for surgical robot with backdrivable capability," *Robot. Comput.-Integr. Manuf.*, vol. 49, pp. 328–334, Feb. 2018.

[9] J. Wang, Z. Qi, and G. Wang, "Hybrid modeling for dynamic analysis of cable-pulley systems with time-varying length cable and its application," *J. Sound Vib.*, vol. 406, pp. 277–294, Oct. 2017.

[10] T.-F. Lee and A.-C. Huang, "Vibration suppression in belt-driven servo systems containing uncertain nonlinear dynamics," *J. Sound Vib.*, vol. 330, no. 1, pp. 17–26, Jan. 2011.

[11] G. Ma, C. Chen, Y. Lyu, and Y. Guo, "Adaptive backstepping-based neural network control for hypersonic reentry vehicle with input constraints," *IEEE Access*, vol. 6, pp. 1954–1966, 2017.

[12] Z. Song and K. Sun, "Adaptive backstepping sliding mode control with fuzzy monitoring strategy for a kind of mechanical system," *ISA Trans.*, vol. 53, no. 1, pp. 125–133, Jan. 2014.

[13] Y. Xia, G. Xu, K. Xu, Y. Chen, X. Xiang, and Z. Ji, "Dynamics and control of underwater tension leg platform for diving and leveling," *Ocean Eng.*, vol. 109, pp. 454–478, Nov. 2015.

[14] Y.-J. Wu, J.-X. Zuo, and L.-H. Sun, "Adaptive terminal sliding mode control for hypersonic flight vehicles with strictly lower convex function based nonlinear disturbance observer," *ISA Trans.*, vol. 71, no. 2, pp. 215–226, Nov. 2017.

[15] S. Butt and H. Aschemann, "Adaptive backstepping control for an engine cooling system with guaranteed parameter convergence under mismatched parameter uncertainties," *Control Eng. Pract.*, vol. 64, pp. 195–204, Jul. 2017.

[16] J. Luo, C. Wei, H. Dai, and J. Yuan, "Robust LS-SVM-based adaptive constrained control for a class of uncertain nonlinear systems with time-varying predefined performance," *Commun. Nonlinear Sci. Numer. Simul.*, vol. 56, pp. 561–587, Mar. 2018.

[17] H. Q. Wang, B. Chen, and C. Lin, "Adaptive neural tracking control for a class of stochastic nonlinear systems with unknown dead-zone," *Int. J. Innov. Comput., Inf. Control*, vol. 9, no. 8, pp. 3257–3269, Apr. 2013.

[18] B. Xu, Z. Shi, C. Yang, and F. Sun, "Composite neural dynamic surface control of a class of uncertain nonlinear systems in strict-feedback form," *IEEE Trans. Cybern.*, vol. 44, no. 12, pp. 2626–2634, Dec. 2014.

[19] L. Sheng, G. Xiaojie, and Z. Lanyong, "Robust adaptive backstepping sliding mode control for six-phase permanent magnet synchronous motor using recurrent wavelet fuzzy neural network," *IEEE Access*, vol. 5, pp. 14502–14515, 2017.

[20] X. Xiang, C. Yu, and Q. Zhang, "On intelligent risk analysis and critical decision of underwater robotic vehicle," *Ocean Eng.*, vol. 140, pp. 453–465, Aug. 2017.

[21] Y. Xia, K. Xu, Y. Li, G. Xu, and X. Xiang, "Modeling and three-layer adaptive diving control of a cable-driven underwater parallel platform," *IEEE Access*, vol. 6, pp. 24016–24034, 2018.

[22] X. Xiang, C. Liu, H. Su, and Q. Zhang, "On decentralized adaptive full-order sliding mode control of multiple UAVs," *ISA Trans.*, vol. 71, pp. 196–205, Nov. 2017.

[23] H. Han, J. Chen, and H. R. Karimi, "State and disturbance observers-based polynomial fuzzy controller," *Inf. Sci.*, vols. 382–383, pp. 38–59, Mar. 2017.

[24] D. Ginoya, P. D. Shendge, and S. B. Phadke, "Disturbance observer based sliding mode control of nonlinear mismatched uncertain systems," *Commun. Nonlinear Sci. Numer. Simul.*, vol. 26, nos. 1–3, pp. 98–107, Sep. 2015.

[25] L. Zhou, Z. Che, and C. Yang, "Disturbance observer-based integral sliding mode control for singularly perturbed systems with mismatched disturbances," *IEEE Access*, vol. 6, pp. 9854–9861, 2018.

[26] B. Fu, Q. Wang, and W. He, "Nonlinear disturbance observer-based control for a class of port-controlled hamiltonian disturbed systems," *IEEE Access*, vol. 6, pp. 50299–50305, 2018.

[27] J. Zhang, C. Sun, R. Zhang, and C. Qian, "Adaptive sliding mode control for re-entry attitude of near space hypersonic vehicle based on backstepping design," *IEEE/CAA J. Automatica Sinica*, vol. 2, no. 1, pp. 94–101, Jan. 2015.

[28] Q. Qu, H. Zhang, R. Yu, and Y. Liu, "Neural network-based H_∞ sliding mode control for nonlinear systems with actuator faults and unmatched disturbances," *Neurocomputing*, vol. 275, pp. 2009–2018, Jan. 2018.

[29] C. Liu, C. C. Cheah, and J.-J. E. Slotine, "Adaptive task-space regulation of rigid-link flexible-joint robots with uncertain kinematics," *Automatica*, vol. 44, no. 7, pp. 1806–1814, Jul. 2008.

[30] S. Pashaei and M. Badamchizadeh, "A new fractional-order sliding mode controller via a nonlinear disturbance observer for a class of dynamical systems with mismatched disturbances," *ISA Trans.*, vol. 63, pp. 39–48, Jul. 2016.

[31] D. Ginoya, P. D. Shendge, and S. B. Phadke, "Sliding mode control for mismatched uncertain systems using an extended disturbance observer," *IEEE Trans. Ind. Electron.*, vol. 61, no. 4, pp. 1983–1992, Apr. 2014.

[32] M. K. Talkhoncheh, M. Shahrokhi, and M. R. Askari, "Observer-based adaptive neural network controller for uncertain nonlinear systems with unknown control directions subject to input time delay and saturation," *Inf. Sci.*, vols. 418–419, pp. 717–737, Dec. 2017.

[33] R. Li, M. Chen, and Q. Wu, "Adaptive neural tracking control for uncertain nonlinear systems with input and output constraints using disturbance observer," *Neurocomputing*, vol. 235, pp. 27–37, Apr. 2017.

[34] T.-S. Li, D. Wang, G. Feng, and S.-C. Tong, "A DSC approach to robust adaptive NN tracking control for strict-feedback nonlinear systems," *IEEE Trans. Syst., Man, Cybern. B. Cybern.*, vol. 40, no. 4, pp. 915–927, Jun. 2010.

[35] D. Swaroop, J. K. Hedrick, P. P. Yip, and J. C. Gerdes, "Dynamic surface control for a class of nonlinear systems," *IEEE Trans. Autom. Control*, vol. 45, no. 10, pp. 1893–1899, Oct. 2000.

[36] M. Chen, G. Tao, and B. Jiang, "Dynamic surface control using neural networks for a class of uncertain nonlinear systems with input saturation," *IEEE Trans. Neural Netw. Learn. Syst.*, vol. 26, no. 9, pp. 2086–2097, Sep. 2015.

[37] A.-C. Huang and Y.-C. Chen, "Adaptive multiple-surface sliding control for non-autonomous systems with mismatched uncertainties," *Automatica*, vol. 40, no. 11, pp. 1939–1945, Nov. 2004.

[38] M. Chen and S. S. Ge, "Adaptive neural output feedback control of uncertain nonlinear systems with unknown hysteresis using disturbance observer," *IEEE Trans. Ind. Electron.*, vol. 62, no. 12, pp. 7706–7716, Dec. 2015.

[39] X. Bu, X. Wu, M. Tian, J. Huang, R. Zhang, and Z. Ma, "High-order tracking differentiator based adaptive neural control of a flexible air-breathing hypersonic vehicle subject to actuators constraints," *ISA Trans.*, vol. 58, pp. 237–247, Sep. 2015.

[40] X. Zhang, X. L. Huang, H. Q. Lu, and Z. G. Yu, "Mapping filtered forwarding-based robust adaptive control for uncertain nonlinear systems with input constraint," *Int. J. Adapt. Control Signal Process.*, vol. 32, no. 2, pp. 248–264, Oct. 2017.

[41] R. Cui, X. Zhang, and D. Cui, "Adaptive sliding-mode attitude control for autonomous underwater vehicles with input nonlinearities," *Ocean Eng.*, vol. 123, pp. 45–54, Sep. 2016.

[42] M. Chen, S. S. Ge, and Y. S. Choo, "Neural network tracking control of ocean surface vessels with input saturation," in *Proc. IEEE Int. Conf. Automat. Logistics*, Shenyang, China, Aug. 2009, pp. 85–89.

[43] S. Galeani, S. Tarbouriech, M. Turner, and L. Zaccarian, "A tutorial on modern anti-windup design," *Eur. J. Control*, vol. 15, nos. 3–4, pp. 418–440, May 2009.

[44] L. Chen, Y.-W. Wang, W. Yang, and J.-W. Xiao, "Robust consensus of fractional-order multi-agent systems with input saturation and external disturbances," *Neurocomputing*, vol. 303, pp. 11–19, Aug. 2018.

[45] M. Chen and B. Jiang, "Adaptive control and constrained control allocation for overactuated ocean surface vessels," *Int. J. Syst. Sci.*, vol. 44, no. 12, pp. 2295–2309, Apr. 2012.

[46] H.-G. Han, Y.-N. Guo, and J.-F. Qiao, "Self-organization of a recurrent RBF neural network using an information-oriented algorithm," *Neurocomputing*, vol. 225, pp. 80–91, Feb. 2017.

[47] J. Park and I. W. Sandberg, "Universal approximation using radial-basis-function networks," *Neural Comput.*, vol. 3, no. 2, pp. 246–257, Jun. 1991.

YINGKAI XIA (M'19) was born in Henan, China, in 1989. He received the B.S. and Ph.D. degrees in naval architecture and ocean engineering from the Huazhong University of Science and Technology, Wuhan, China, in 2011 and 2017, respectively.

In 2018, he was a Visiting Scholar with the School of Mechanical Engineering, The University of Adelaide, Australia. He holds a Postdoctoral position with the School of Naval Architecture, Ocean and Civil Engineering, Shanghai Jiao Tong University. He is also with the Underwater Vehicle Researching Team, School of Naval Architecture and Ocean Engineering, Huazhong University of Science and Technology. He is also with the Underwater Vehicle Researching Team, School of Naval Architecture and Ocean Engineering, Huazhong University of Science and Technology. His current research interests include design of underwater equipment, dynamic modeling and adaptive control of complex nonlinear systems, renewable energy technology, and ocean engineering.

KAN XU was born in Hubei, China, in 1990. She received the B.S. degree in control science and engineering and the M.S. degree in naval architecture and ocean engineering from the Huazhong University of Science and Technology, Wuhan, China, in 2011 and 2014, respectively.

She is currently an Engineer with the Wuhan Second Ship Design and Research Institute. Her current research interests include design of underwater vehicle, intelligent control of complex nonlinear systems, and system development.

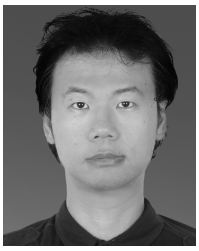

YE LI (M'98–SM'10) was born in Beijing, China, in 1977. He received the B.S. degree in naval architecture and ocean engineering from Shanghai Jiao Tong University, Shanghai, China, in 2000, and the M.S. and Ph.D. degrees in mechanical engineering from The University of British Columbia, Canada, in 2004 and 2007, respectively.

From 2007 to 2009, he was a Research Assistant with the Energy Technology Division, Advanced Power and Energy System Group, Pacific Northwest National Laboratory, USA. From 2009 to 2013, he was a Senior Research Scientist and the Founding Lead of the National Wind Technology Center, Offshore Energy Modeling Group, National Renewable Energy Laboratory, USA. He is currently a Professor with the School of Naval Architecture, Ocean and Civil Engineering, Shanghai Jiao Tong University, the Director of Shanghai Jiao Tong University, multiple functional towing tank, and the Director of the NRDC National Center for Offshore Wind Technology. His current research interests include marine hydrodynamics, renewable energy technology, and mathematical modeling of complex systems.

GUOHUA XU was born in Hubei, China, in 1964. He received the B.S. and M.S. degrees in automation from the Wuhan University of Technology, Wuhan, China, in 1986 and 1991, respectively, and the Ph.D. degree in mechatronic engineering from the Huazhong University of Science and Technology, Wuhan, in 2005.

From 1986 to 1991, he was a Research Assistant with the Wuhan University of Technology. He is currently a Professor and the Deputy Dean of the School of Naval Architecture and Ocean Engineering, Huazhong University of Science and Technology, the Deputy Director of Hubei Ships and Marine hydrodynamics Key Laboratory, and the Director of the Institute of Intelligent Machinery and Control. His research interests include complex marine system development, underwater operation, intelligent control of underwater vehicle, and ocean engineering.

XIANBO XIANG (S'09–M'12) was born in Hubei, China, in 1978. He received the B.S. and M.S. degrees in automatic control and marine engineering from the Huazhong University of Science and Technology, China, in 2000 and 2003, respectively, and the Ph.D. degree in robotics from the University of Montpellier 2, Montpellier, France, in 2011.

In 2006, he was an EC Erasmus Mundus Visiting Scholar with the SpaceMaster Project. From 2008 to 2011, he worked for the European Project FreeSubNet as an EC Marie Curie ESR Fellow at LIRMM, CNRS UMR 5506, France. He is currently a Professor and the Deputy Dean of the School of Naval Architecture and Ocean Engineering, Huazhong University of Science and Technology. His research interests include nonlinear control of nonholonomic mobile robot and underactuated autonomous underwater vehicles, and coordinated control of multiple autonomous vehicles.